Phospholipids in motion: High Resolution ^{31}P NMR Field Cycling Studies

Mary F. Roberts,[1,*] Jingfei Cai,[1] V. N. Sivanandam,[2] Hanif M. Khan,[3] Nathalie Reuter[3], Anne Gershenson,[4] and Alfred G. Redfield[2]

[1]Department of Chemistry, Boston College, Chestnut Hill, Massachusetts 02467

[3]Department of Biochemistry and the Rosenstiel Basic Medical Sciences Research

Institute, Brandeis University, Waltham, Massachusetts 02454

[4]Department of Molecular Biology and Computational Biology Unit, Department of Informatics,

University of Bergen, Bergen, Norway

[5]Department of Biochemistry and Molecular Biology, University of Massachusetts, Amherst,

Massachusetts

[6]Department of Biochemistry, Brandeis University, deceased July 24, 2019

1

ABSTRACT

Diverse phospholipid motions are key to membrane function but can be quite difficult to untangle and quantify. High resolution field cycling ^{31}P NMR spin-lattice relaxometry, where the sample is excited at high field, shuttled in the magnet bore for low field relaxation, then shuttled back to high field for readout of the residual magnetization, provides data on phospholipid dynamics and structure. This information is encoded in the field dependence of the ^{31}P spin-lattice relaxation rate (R_1). In the field range from 11.74 down to 0.003 T three dipolar nuclear magnetic relaxation dispersions (NMRDs) and one due to ^{31}P chemical shift anisotropy contribute to R_1 of phospholipids. Extraction of correlation times and maximum relaxation amplitudes for these NMRDs provides (1) lateral diffusion constants for different phospholipids in the same bilayer, (2) estimates of how additives alter the motion of the phospholipid about its long axis, and (3) an average ^{31}P – ^{1}H angle with respect to the bilayer normal, which reveals that polar head group motion is not restricted on a μs timescale. Relative motions within a phospholipid are also provided by comparing ^{31}P NMRD profiles for specifically deuterated molecules as well as ^{13}C and ^{1}H field dependence profiles to that of ^{31}P. Although this work has dealt exclusively with phospholipids in small unilamellar vesicles, these same NMRDs can be measured for phospholipids in micelles and nanodiscs, making this technique useful for monitoring lipid behavior in a variety of structures and assessing how additives alter specific lipid motions.

INTRODUCTION

As critical structural components of membranes phospholipids are characterized by complex motions that occur on widely different time and length scales.[1] These include motions ascribed to an individual phospholipid such as acyl chain isomerizations (~1 to 10 ps), wobbling of an individual molecule about its long axis (~ 10 ns) and lateral diffusion (0.1 to 10 μs) in the membrane, as well as cooperative motions leading to macroscopic motions (e.g., bilayer undulations or bending). The polar headgroups of phospholipids can provide specific binding sites for peripheral membrane proteins whose transient interactions physically alter membrane properties (e.g., cardiolipin interactions with apoptosis effectors in mitochondria[2]) or whose enzymatic activity modifies membrane composition (e.g., hydrolysis of specific phosphoinositides by phospholipase C enzymes to generate second messengers[3]). Defining specific phospholipid-protein interactions is clearly important, but understanding how bilayer dynamics respond to the binding of proteins or other additives is also necessary.

For phospholipids, ^{31}P NMR dynamics, as reflected in relaxation rates, can provide a description of motions sensed by the polar headgroup. A good example is the work of Dufourc and co-workers who carried out various ^{31}P relaxation experiments on multilamellar oriented and unoriented dimyristoylphosphatidylcholine to assess the contribution of specific phospholipid motions.[4] Phosphorus interactions with nearby protons dominate the ^{31}P spin-lattice relaxation rate (R_1) except at high fields (> 6T), where chemical shift anisotropy (CSA) relaxation begins to dominate.[5] However, different types of motion and different relaxation mechanisms can contribute to the observed ^{31}P R_1 at a given field, complicating the interpretation of R_1.

The variation of R_1 with Larmor frequency, proportional to magnetic field, has the potential to separate different nuclear magnetic relaxation dispersions (NMRDs). Proton 'fast field cycling' (FFC) relaxometry covers a wide range of magnetic fields with fast electromagnets (a recent volume of *New Developments in NMR* provides a wealth of information on many aspects and uses of this technique[6]). For phospholipid bilayers FFC has been used to identify many NMRDs over a much larger motional time-scale than is available with fixed field NMR experiments.[7,8] However, there is no chemical shift discrimination in these ^1H experiments, and the motions attributed to the different dipolar NMRDs are assigned by modeling different motions to assess how they fit the data. Sensitivity also decreases as the field is decreased, making such a technique less useful for ^{31}P or ^{13}C. One way to avoid large losses in sensitivity and to maintain separated chemical shifts is to excite the sample at high field, mechanically move (shuttle) the sample to a lower field where it can relax, then return it to the static high field for readout. Pioneering work in ^1H shuttling relaxometry has been carried out by R. G. Bryant and coworkers using a spectrometer with two magnetically isolated independent magnets and pneumatic shuttling.[9-11] Another type of shuttling field cycling that has been very useful for ^{31}P, particularly in systems with multiple phosphorus containing molecules, uses a stepper motor drive instead of a pneumatic drive and an extra coil above the superconducting magnet to reach down to 0.003 T.[12]

For phospholipids, multiple $^{31}P - {}^1H$ dipolar NMRDs have been detected between 0.003 and 11.74 T.[5,13,14] While correlation times are easily extracted, identification of the motions responsible for each NMRD and which nearby protons contribute to the ^{31}P R_1 of different nearby protons has been incomplete to date. The results reported here address those issues. We separate the

contribution of choline and glycerol O-methylenes to the ^{31}P R_1 of phosphatidylcholine (PC) in SUVs using selectively deuterated phospholipids. Separation of the R_1 amplitude and correlation time for the glycerol and choline (or other esterified alcohol) ^{31}P interaction with the O-methylene protons provides an effective distance between the ^{31}P and the protons relaxing it (r_{P-H}) that reflects changes in dihedral angle on a 10 ns timescale. A comparison of ^{31}P correlation times with field-dependent R_1 profiles for ^{13}C and ^{1}H nuclei in other parts of a PC molecule provides a more complete picture of phospholipid motions in these small vesicles. In particular, dipolar correlation times for the field cycling profiles of different nuclei bolster the idea of treating the phospholipid as a wobbling cylinder in a membrane (at least on timescales above 1 ns)[14], and also indicate that a third dipolar NMRD with a sub-nanosecond correlation time exists in the ^{31}P profile but is partially obscured by the CSA relaxation. Assignment of ^{31}P–^{1}H dipolar NMRDs to these specific motions then provides more detailed insights into specific phospholipid/protein and phospholipid/cholesterol interactions.

EXPERIMENTAL METHODS

Chemicals. Dipalmitoylphosphatidylcholine (DPPC), (1-palmitoyl-2-oleoyl-PC (POPC), dioleoylphosphatidic acid (DOPA), dioleoylphosphatidylmethanol (DOPMe)) and d$_{75}$-dipalmitoyl-PC (d$_{75}$-DPPC) were obtained from Avanti Polar Lipids and used without further purification. [1-^{13}C]palmitic acid and [1-^{13}C]oleic acid were obtained from Cambridge Isotopes, Inc. Structures of isotopically labeled phospholipids are shown in Figure S1. The *sn-2* ^{13}C-carbonyl labeled POPC, PO[1-^{13}C]PC, was previously synthesized from 1-palmitoyl-PC and [1-^{13}C]oleic acid.[15] POPC with the *sn-1* carbonyl labeled, P[1-^{13}C]OPC, was synthesized in three steps: (i) acylation of *sn*-glycerol-3-phosphocholine with [1-^{13}C]-palmitic acid; (ii) removal of the *sn*-2 palmitic acid by bee venom phospholipase A$_2$, and (iii) reacylation of the resulting lyso-PC with unlabeled palmitic acid. Further comments on the synthesis and purity of the ^{13}C labeled POPC are provided in the Supplemental Material.

Vesicle preparation. Small unilamellar vesicles (SUVs) (with a total phospholipid concentration of 5 or 10 mM) were prepared by sonication of lipid suspensions in buffer containing 20-40% D$_2$O, and 5 mM EDTA, at a pH of 7.5 unless otherwise indicated. The buffers were 50 mM Tris chloride or sodium borate (for ^{31}P), and 20 mM phosphate for ^{13}C and ^{1}H (to avoid the natural abundance ^{13}C or ^{1}H resonances from the Tris buffer). SUVs with free [1-^{13}C]oleic acid (5 mM) and POPC (20 mM) with 1 mM EDTA and 25 mM HEPES, pH 7.5 were also used. The average diameter of these sonicated vesicles was typically 250 Å with 90% of the sizes between 200 and 400 Å as determined by dynamic light scattering.[16] For the DPPC and d$_{75}$-DPPC samples, the dry phospholipid was suspended in buffer and the sample was sonicated above 40°C. The sample was then allowed to sit for several hours at room temperature before being sealed in the NMR tube. Incubation below the T_m induces fusion resulting in large unilamellar vesicles (LUVs), averaging around 1000 Å in diameter.

Field cycling NMR relaxometry experiments and data analysis. ^{31}P, ^{13}C, and ^{1}H spin-lattice relaxation rates (R_1) were measured in a Varian Inova 500 NMR with a mechanized shuttle system mounted on its top.[12] The pulse sequence for obtaining R_1 has been described previously.[17] Samples and susceptibility plugs were epoxied into special NMR tubes adapted for use with the shuttler. ^{31}P and ^{13}C data were typically acquired over a 3-4 day period for a full field-dependence

profile (11.6 down to 0.003 T). Experiments were usually run at 25°C. Vesicles composed of DPPC and d_{75}-DPPC were run at 44°C and 39°C respectively; chain perdeuteration has been shown to lead to a 5° drop in the T_m for d_{62}-DPPC compared to DPPC.[18] The spin lattice relaxation rate (R_1) at each magnetic field (B_{relax}), shown as the angular frequency ω_j for the nucleus of interest, j, in most of the figures (e.g., for ^{31}P, $\omega_P = \gamma_P B_{relax}$ where $\gamma_P = 1.083 \times 10^8$ rad s^{-1}), was measured using 6-8 programmed delay times. The data were fit to a single exponential function versus delay time in order to extract R_1 at each relaxation field/Larmor frequency. For each sample at least three fields (typically 5, 0.1, and 0.01 T) were repeated. The R_1 values for duplicate fields were within the uncertainty of the fit, with the latter the error bars shown on each lot.

An example of the ^{31}P R_1 data obtained is shown in Figure 1 for POPC (5 mM) in SUVs with an equimolar amount of d_3-DOPMe. Both the magnetic field and the Larmor frequency scales for relaxation are displayed.
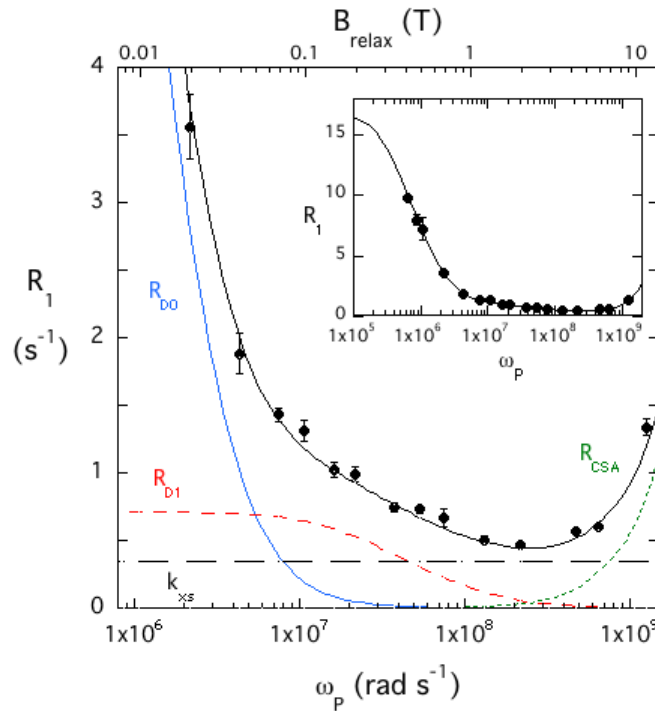

Figure 1. The magnetic field and Larmor frequency dependence of R_1 for POPC (5 mM) in SUVs with d_3-DOPMe (5 mM). The observed NMRDs result from two previously identified dipolar relaxation mechanisms, R_{D0} (blue solid line) and R_{D1} (red line with long dashes), and the CSA relaxation at high frequencies (R_{CSA}, green line with short dashes). There is 'excess R_1' that is treated as a constant (k_{xs}, black dashed horizontal line) here. The inset expands the R_1 scale for an estimation of $R_{D0}(0)$, the R_1 extrapolated to zero field.

Dipole-dipole coupling (R_{Di}) as well as ^{31}P CSA (R_{CSA}) contribute to experimental ^{31}P R_1 of the phospholipid as follows.

$$R_{Di} = R_{Di}(0)\{0.1/(1+ (\omega_H - \omega_P)^2 \tau_{Di}^2) + 0.3/(1+ \omega_P^2 \tau_{Di}^2) + 0.6/(1+(\omega_H + \omega_P)^2 \tau_{Di}^2)\} \qquad [1]$$
$$i = 0, 1, \text{ or } 2 \text{ for } R_{D0}, R_{D1}, R_{D2}$$

$$R_{CSA} \simeq k_{CSA} \omega_P^2 \qquad (k_{CSA} \text{ is a constant}) \qquad [2]$$

5

In this work, the relevant parameters extracted directly from the data for each NMRD are the dipolar correlation time (τ_{Di}) and the maximum relaxation rate ($R_{Di}(0)$). The addition of R_{CSA} is important for fitting the ^{31}P data, but not useful otherwise because we cannot estimate a correlation time for this mechanism.

The two obvious contributions from $^1H - {}^{31}P$ dipole coupling to the POPC ^{31}P relaxation are R_{D0}, easily seen below $5x10^6$ rad s^{-1} ($B_{relax} \sim 0.05$ T, inset in Figure 1) and R_{D1}, which begins to increase below 10^8 rad s^{-1} ($B_{relax} \sim 1$ T) (Figure 1). R_{D1} reaches its maximum rate a little below 10^7 rad s^{-1} (~0.08 T) and is a constant contribution to R_1 at lower fields. For ^{31}P, R_{D0} has a correlation time ~ 0.5 µs that is faster than the correlation time for tumbling of these small vesicles.[13] A similar correlation time is seen with FFC studies of vesicles,[7,8] and has been attributed to a relaxation from vesicle reorientation (rotation) that is aided by translational displacements of phospholipids.

The τ_{D1} correlation time was originally suggested to derive from axial rotation of the phospholipid in the bilayer,[5] a motion better described as small lateral movements of an individual phospholipid in a cluster of molecules that effectively rotate it. A different interpretation of the dipolar relaxation on this time-scale is that it arises from restricted 'wobble in a cone' of the long axis of the phospholipid in the bilayer.[14] This model is based on the key assumption that fast internal motions lead to an average phospholipid molecular shape well fit by a cylinder when the time scale is on the order of 10 ns (Figure S1). Wobbling would affect chain and backbone behavior and potentially the polar headgroup as well (depending on its internal mobility). The R_{D1} frequency region is useful for estimating the effective $^{31}P - {}^1H$ distance for the dipolar interaction since $\tau_{D1}/R_{D1}(0)$ is proportional to $r_{PH}{}^6$ as shown in Equation [3].[5,14]

$$r_{PH}{}^6 = (\tau_{D1}/R_{D0}) \ (\ \mu_0/4\pi)^2 \ (h/2\pi)^2 \ \gamma_P{}^2 \ \gamma_H{}^2 \qquad [3]$$

Here μ_0 is the magnetic permeability in a classical vacuum, while γ_P and γ_H are the gyromagnetic ratios for ^{31}P and ^1H, respectively. This formula assumes a single $^{31}P - {}^1H$ interaction and a fixed geometry that does not vary with time. However, for a phospholipid ^{31}P, the number of protons contributing to its relaxation is not necessarily known, and distances will vary with changes in dihedral angles. Comparisons of $\tau_{D1}/R_{D1}(0)$ for a system under different conditions can detect changes in motion or number of protons contributing to the ^{31}P relaxation.

There is also a region around 2-4 T where R_1 is higher than what is predicted for by $R_{D0}+R_{D1}+R_{CSA}$. Two mechanisms that could produce this excess R_1 include (1) cross-correlation relaxation[19], R_{CC}, between R_{D0} and R_{CSA} (Equation 4), or (2) a third dipolar mechanism, R_{D2}, with a very fast correlation time such that we see only $R_{D2}(0)$.

$$R_{CC} = (R_{D0} \ x \ R_{CSA}) = R_{D0}(0)\{1/(1+ \omega_P{}^2 \ \tau_{D0}{}^2)\} x \ k_{CSA} \ \omega_P{}^2 \qquad [4]$$

For these small phospholipid vesicles, τ_{D0} is around 0.5 µs so that above $\omega_P \sim 1x10^7$ rad s^{-1} the R_{CC} contribution would be a constant, $R_{CC} = R_{D0}(0)x \ k_{CSA} /\tau_{D0}{}^2$. At Larmor frequencies $<10^7$ rad s^{-1}, R_{CC} will decrease, but it would contribute little to the much higher R_{D0} at those low frequencies.

If a third dipolar term, R_{D2}, is responsible for the excess R_1 seen in the 2 to 5 $x10^7$ rad s^{-1} range, it should decrease at high frequencies. However, that decrease in R_{D2} could be obscured by R_{CSA}. To

a first approximation, we assume that R_{D2} would be a constant, $R_{D2}(0)$, in the frequency range we are examining.

Thus, both mechanisms are treated as a constant (k_{XS}) in fitting the observed R_1 values. Using k_{XS} for the 'excess' R_1 rather than a second R_{CSA} term (an ad hoc assumption used previously[5]) leads to a slightly longer τ_{D1} and smaller $R_{D1}(0)$ for phospholipids. For example, for the POPC in Figure 1, τ_{D1} is around 10 ns rather than the 5-6 ns for POPC samples when a second R_{CSA} was used instead of k_{xs}.[5, 20]

The ^{31}P R_{D0}, R_{D1}, and R_{CSA} are well separated in ω_P, making it possible to use the sum of the relaxation mechanisms to fit the entire frequency range to obtain τ_{D0}, $R_{D0}(0)$, τ_{D1}, $R_{D1}(0)$, and constants k_{XS} and k_{CSA}. However, it is often better to analyze separately the high field/frequency CSA region to obtain k_{CSA} and the low field/frequency dipolar NMRD to obtain a good estimate for R_{D0} parameters. These contributions can then be subtracted from the experimental R_1 data. Figures 2 shows examples of this approach to extracting R_{D1} parameters by either removing R_{CSA} (Fig. 2B) or R_{D0} (Fig. 2D).

The frequency dependence for ^{13}C was analyzed with the same framework used for ^{31}P by replacing ω_P with ω_C and is similar to what was done in an earlier ^{13}C field cycling study of [1-^{13}C]-benzoic acid, which dimerizes at low temperatures.[21] As seen previously for PO[1-^{13}C]PC,[16] two dipolar terms and a very small CSA term are not adequate for fitting the observed R_1 profile as a function of Larmor frequency ω_C. Therefore, we evaluate the Larmor frequency dependence as $R_1 = R_{D0} + R_{D1} + k_{XS} + R_{CSA}$.

For ^1H R_1 data, dipolar relaxation was analyzed with the expression

$$R_D = R_D(0)\{0.2/(1+\omega_H^2 \tau_H^2) + 0.8/(1+(4 \omega_H^2 \tau_H^2)\} \qquad [5]$$

where $\omega_H = 2.675 \times 10^8$ rad s^{-1} T^{-1} x B_{relax}(T). This expression for R_D is a simplification for the methyl groups, particularly the choline N-methyls, where spin rotation likely dominates the relaxation since the nearest other ^1H atoms are four bonds away. The ^1H R_1 versus ω_H profiles all displayed two NMRDs, so the frequency dependence was treated as the sum of two dipolar terms with different correlation times.

Estimation of ^{31}P -^1H distances and ^{31}P – ^1H vector angles with respect to the bilayer normal

The average P-H distances and the orientation of ^{31}P-^1H groups with respect to the bilayer normal were calculated from the molecular dynamics trajectory of a pure DMPC bilayer.[22] The bilayer consisted of 256 DMPC lipids (128 lipids in each leaflet) and the simulation used the CHARMM36 lipid force field.[23] The simulation was carried out for 500 ns with the last 300 ns analyzed. For each lipid we defined a vector between its phosphorus atom and each relevant hydrogen atom (choline and glycerol -OCH$_2$- groups) within the same lipid. For each frame in the trajectory, the norm of these vectors and their angles with respect to the bilayer normal were calculated for individual lipids and then averaged over all the lipids. The procedure was repeated over the full trajectory and the values for each frame were averaged for reporting. The length and orientation of ^{13}C-^1H vectors were also calculated in a similar manner. The calculations were carried out using

custom TCL scripts and MEMBPLUGIN[24] in VMD[25], and the θ_{PH} or θ_{CH} and r_{PH} or r_{CH} are listed in Table 1 for comparison to values extracted from the field cycling experiments.

Table 1. Average $r_{P(C)-H}$ and $\theta_{P(C)-H}$ for dimyristoylphosphatidylcholine (DMPC) from a molecular dynamics simulation.

Vector	CHARMM atom type [a]	$r_{P(C)-H}$ (Å)	$\theta_{P(C)-H}$ (°)
P-H (choline)	P-H11A	3.09±0.003	90.0±1.9
P-H (choline)	P-H11B	3.09±0.004	90.0±1.9
P-H (glycerol)	P-HA	3.02±0.003	49.7±1.2
P-H (glycerol)	P-HB	3.00±0.002	49.9±1.2
C-H (*sn*-2)	C21-H2R	2.14±0.001	76.8±1.6
C-H (*sn*-2)	C21-H2S	2.15±0.001	72.4±1.6
C-H (*sn*-1)	C31-H2X	2.15±0.001	49.4±1.5
C-H (*sn*-1)	C31-H2Y	2.14±0.001	49.6±1.5

[a] Atom type as identified in an earlier simulation of a DPPC bilayer at a higher temperature.[14]

RESULTS

Polar headgroup protons contribute to phospholipid ^{31}P dipolar relaxation

Early field cycling studies for phosphatidic acid, PA, in vesicles with POPC showed that $\tau_{D1}/R_{D1}(0)$ was very similar to that for PC.[5,20] PA lacks a polar alcohol such as choline, serine, ethanolamine, etc., esterified to the phosphate moiety. Compared to PC one would expect a significantly reduced amplitude for the PA $R_{D1}(0)$ if both glycerol and choline -OCH_2- resonances relax the POPC ^{31}P. A possible explanation for the similarity of the PA τ_{D1}/R_{D1} suggested by MD simulations for DPPC, is that τ_{D1} differs for the two methylene groups and is shorter for the choline methylene whose amplitude would be reduced and the NMRD would be shifted to higher ω_P where CSA relaxation starts to contribute significantly.[14] However, recent studies of PA/PC films and vesicles show PA ionization as well as acyl chain unsaturation can lead to PA/PC complexes stabilized by hydrogen bonds and charge pairs.[26] Such intermolecular complexes could contribute to dipolar relaxation of PA. Thus, a better assessment of whether or not the choline methylene protons contribute to ^{31}P relaxation is to use a PC with a perdeuterated choline moiety.

Figure 2A shows the variation of the ^{31}P R_1 from 10^6 to 2×10^9 rad s^{-1} (roughly 0.01 to 18 T) for DPPC and d_{75}-DPPC. Since perdeuteration of the acyl chains has been shown to reduce the gel-to-liquid crystalline phase transition of saturated chain phospholipids, the samples were run at slightly different temperatures, 44°C for DPPC and 39°C for d_{75}-DPPC. This adjustment should ensure comparable bilayer fluidity. The observed R_1 values above 10^6 rad s^{-1} have contributions from R_{D1}, R_{CSA}, and k_{XS} (Figure 2A). The data above 3×10^8 rad s^{-1} were fit by treating R_1 as $k_{XS} + k_{CSA}\omega_P^2$. The extracted k_{CSA} can be used to subtract the R_{CSA} component from the observed R_1 yielding the frequency dependence profile in Figure 2B. Analysis of ΔR_1, the sum of R_{D1} and k_{XS}, yields the τ_{D1}

and $R_{D1}(0)$ values seen in Table 2. τ_{D1} is the same within errors for the two PC samples, while $R_{D1}(0)$ is reduced two-fold when the choline is perdeuterated. The k_{XS} is also decreased about two-fold. The values of τ_{D1} and $R_{D1}(0)$ for d_{75}-DPPC can be used to subtract the contribution of the glycerol methylene from the DPPC ^{31}P R_1 (Figure S2). Analysis of the resultant R_1 values yields a τ_{D1} of 16±5 ns for the choline methylene contribution that is comparable to the value for the glycerol methylene interaction (25±8 ns). Thus, the two ^{31}P-O-C-H_2 interactions appear to have similar τ_{D1} values and both methylene groups contribute equally to the DPPC dipolar ^{31}P R_1 of the R_{D1}.
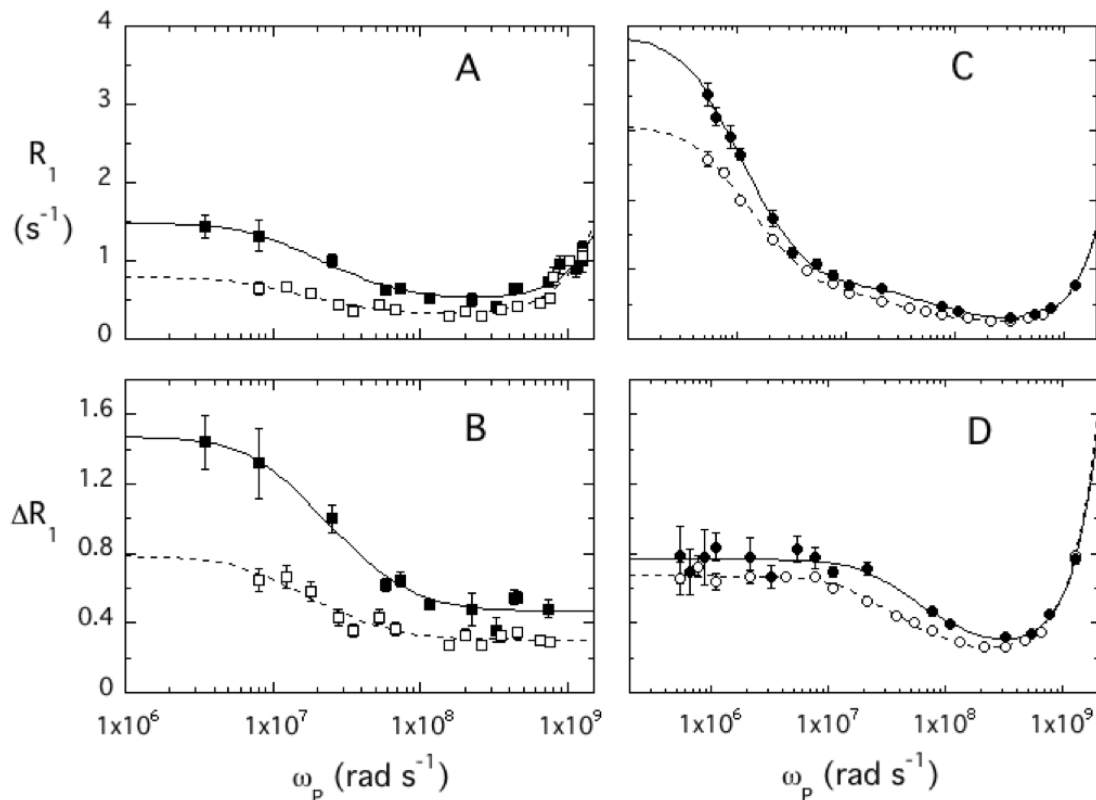

Figure 2. Effect of phospholipid polar headgroup deuteration of ^{31}P R_1 as a function of ω_P. (A) The R_1 profiles for vesicles of DPPC (filled circle) or d_{75}-DPPC (empty circle) are shown. The DPPC vesicles were run at 44°C while its perdeuterated counterpart was run at 39°C. (B) The ΔR_1 profile for DPPC or d_{75}-DPPC is shown after subtraction of the R_{CSA} term ($\Delta R_1 = R_{D1} + k_{xs}$). (C) R_1 for DOPMe (filled square) or d_3-DOPMe (empty square) in SUVs as a function of ω_p. (D) ΔR_1 for the data in (C) after subtracting the R_{D0} component from the DOPMe and d_3-DOPMe R_1 values in (C), where $\Delta R_1 = R_{D1}+k_{XS}+R_{CSA}$. The temperature for the DOPMe and d_3-DOPMe experiments was 25°C.

If we normalize $R_{D1}(0)$ by the number of proton relaxers, the distance estimated from $\tau_{D1}/R_{D1}(0)$ should be the same for both proteo- and deutero-DPPC. The normalized r_{PH} values per proton are 4.4 and 4.6 Å for DPPC and d_{75}-DPPC, respectively, indicating that the two methylene groups relax the ^{31}P to the same extent. In simulations of DPPC at 50° C [14] and the DMPC at 27°C [22], r_{PH} for the methylene protons was 3.0-3.1 Å. However, each ^{31}P-O-C-^{1}H dihedral angle and r_{PH} can vary on a time-scale faster than R_{D1}. To account for the longer than expected average r_{PH}, an order parameter, S_D^2, could be introduced to reduce $R_{D1}(0)$.[5] If that is done using the 3 Å value from the simulation as the actual average r_{PH}, S_D^2 is estimated as 0.09.

9

Table 2. Phospholipid dipolar ^{31}P, ^{13}C, and ^{1}H τ_i and $R_{Di}(0)$ values extracted from the frequency dependence of the longitudinal relaxation rate R_1. [a]

	nucleus	τ_{D0} (μs)	$R_{D0}(0)$ (s^{-1})	τ_{D1} (ns)	$R_{D1}(0)$ (s^{-1})	$\tau_{D1}/R_{D1}(0)$ (s^2)	τ_{D2} (ns)	k_{XS} (s^{-1})
POPC [b]	^{31}P	0.59±0.05	15.8±0.9	10±3	0.71±0.11	1.4×10^{-8}		0.4±0.1
DPPC [c]	^{31}P	–	–	19±3	1.00±0.06	1.9×10^{-8}		0.46±0.03
d$_{75}$-DPPC [c]	^{31}P	–	–	25±8	0.48±0.09	5.2×10^{-8}		0.30±0.02
DOPMe	^{31}P	0.40±0.03	3.6±0.1	7±2	0.53±0.08	1.3×10^{-8}		0.24±0.08
d$_3$-DOPMe	^{31}P	0.35±0.02	2.4±0.1	12±1	0.45±0.02	2.7×10^{-8}		0.22±0.01
P[1-^{13}C]OPC [d]	^{13}C	0.72±0.11	48±8	4 ±2 [e]	0.70±0.12 [e]	0.6×10^{-8}	–	0.4±0.1
PO[1-^{13}C]PC [d]	^{13}C	1.5±0.3	16±3	17±2 [e]	2.5±0.1 [e]	0.7×10^{-8}	–	0.40±0.06
[1-^{13}C]oleate [f]	^{13}C	0.52±0.07	10.4±0.5	5.0±2.3 [e]	0.34±0.06 [e]	1.5×10^{-8}		0.23±0.05
POPC/DOPMe [b]								
-N(CH$_3$)$_3$	^{1}H	0.33±0.07	8.6±1.2	–	–	–	0.35±0.08	4.4±0.3 [g]
-(CH$_2$)$_n$-	^{1}H	–	–	21±8	7.5±1.0	0.28×10^{-8}	0.3±0.2	3.8±0.9 [g]
ω-CH$_3$	^{1}H	–	–	14±4	6.7±0.6	0.21×10^{-8}	0.2±0.1	2.6±0.5 [g]

[a] Unless otherwise noted, the parameters were from fitting the entire Larmor frequency range ($R_1 = R_{D0} + R_{D1} + k_{xs} + R_{CSA}$).
[b] These POPC SUVs have an equimolar amount of d$_3$-DOPMe.
[c] The DPPC LUV sample was run at 44°C; the d$_{75}$-DPPC LUV sample was run at 39°C. For these larger vesicles, there would be insufficient R_1 data to measure R_{D0} parameters, hence data were only acquired above $\omega_P = 10^6$ rad s^{-1} and the fit was to $R_{D1} + k_{SX} + R_{CSA}$.
[d] Vesicles of equal molar ^{13}C-labeled POPC and DOPMe, pH 7.5.
[e] The R_{D1} parameters were determined by subtracting the R_{D1} contribution and fitting ΔR_1 with $R_{D1} + k_{xs}$. Data only up to 6×10^8 rad s^{-1} were used to avoid the small R_{CSA} rise.
[f] Vesicles of POPC and [1-^{13}C]oleate/POPC (1:4), pH 7.5.
[g] In the ^{1}H experiments, k_{xs} is $R_{D2}(0)$.

Single component SUVs of either DOPMe or d$_3$-DOPMe (where the methoxy group attached to the ^{31}P has been deuterated, -OCD$_3$) were also examined. To isolate the R_{D1} mechanism, the τ_{D0} and R_{D0} obtained from fitting the low field region were used to subtract R_{D0} from the observed R_1. Then ΔR_1 was analyzed as $R_{D1} + k_{XS} + k_{CSA}$ (Figure 2D). The substitution of the deuterated methyl group decreased $R_{D1}(0)$ about 15% while τ_{D1} increased 1.7-fold , both terms leading to an overall two-fold increase in the ratio $\tau_{D1}/R_{D1}(0)$ (Table 3). Thus, for DOPMe, both the glycerol -OCH$_2$- and the polar headgroup (–OCH$_3$) protons relax the ^{31}P. The increased τ_{D1} indicates that the glycerol ^{31}P-O-CH$_2$ vectors reorient more slowly than the head group ^{31}P-O-CH$_3$.

The question remains as to why vesicles of PA exhibited a high $R_{D1}(0)$ in the original observations of POPA/POPC SUVs[5] and DOPA/POPC SUVs[20] in 50 mM MES, pH 7.5. The pK$_{A2}$ of DOPA (deprotonation of the monoanion to the dianion) is lowered by the presence of the PC.[26,27] The choice of buffer can also affect the PA pK$_{A2}$ (Figure S3) in a similar fashion to PC. With the addition of PC, the reduction of pK$_{A2}$ could be caused by a reduction in the negative surface charge

making deprotonation easier (consistent with the larger shift in pK_{A2} occurring for PA in the inner leaflet), or by formation of transient POPC/DOPA complexes.[26]

DOPA $^{31}P - ^1H$ dipolar interactions were further explored with DOPA SUVs using 50 mM buffer to supply either an organic cation (Tris) or Na^+. As shown in Figure 3, the DOPA R_1 is higher in Tris than in borate buffer between $3x10^6$ and $3x10^8$ rad s^{-1}. However, it is hard to extract a τ_{D1} since for these small vesicles τ_{D0} is ~ 0.3 µs and R_{D0} overlaps the low frequency end of R_{D1}. The τ_{D0} and $R_{D0}(0)$ could be estimated separately using only low field data, then subtracted from the DOPA R_1 values for each sample. A plot of the resultant ΔR_1 versus ω_P has three NMRD components: $R_1 + k_{XS} + R_{CSA}$ (Figure 3 inset). The τ_{D1} for DOPA in Tris (4.0 ± 1.8 ns) is reduced when compared to that lipid in borate buffer ($\tau_{D1} = 9.4\pm1.6$ ns) while the $R_{D1}(0)$ values are the same (0.51 ± 0.10 and 0.54 ± 0.04 for DOPA in Tris and borate, respectively). For DOPA in Tris, the $\tau_{D1}/R_{D1}(0)$ is smaller than the value for that lipid in borate, indicating that transient interactions of the DOPA with the soluble Tris cation contribute to R_{D1}. If the high concentration of Tris cation used as a buffer contributes to dipolar relaxation of the DOPA ^{31}P, then so could the choline moiety of POPC in the same vesicles with the DOPA.
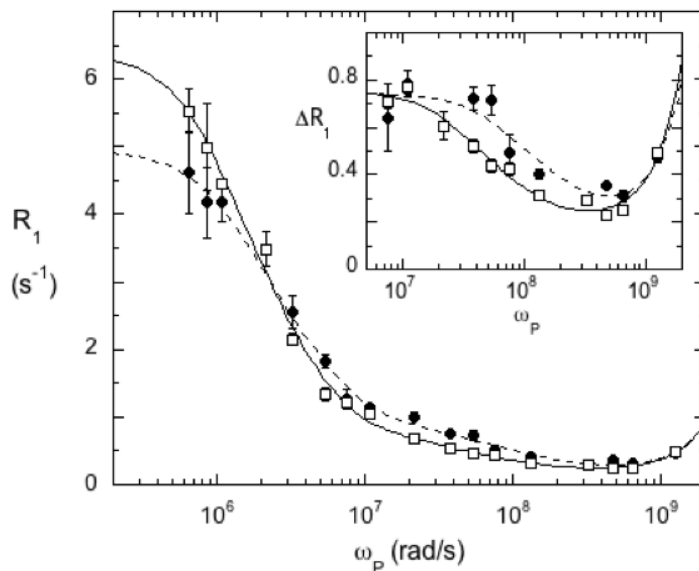

Figure 3. Frequency dependence of the ^{31}P R_1 for DOPA (5 mM) SUVs in 50 mM Tris chloride (circles) or 50 mM sodium borate (squares). The inset, ΔR_1 with R_{D0} subtracted from the observed R_1, shows that the τ_{D1} for DOPA in Tris is shorter than that in borate. Both buffers were at pH 7.5; experiments were carried out at 25°C.

2. Dipolar relaxation of ^{13}C-labeled carbonyls of POPC shows dynamic differences

Analysis of R_1 profiles for the two carbonyl carbons of the phospholipid as a function of relaxation Larmor frequency make an interesting contrast to those of ^{31}P. Shown in Figure 4A is the ^{13}C R_1 for P[1-^{13}C]OPC, where, the *sn*-1 palmitoyl carbonyl is ^{13}C enriched. The profile for the *sn*-2 labeled carbonyl carbon, PO[1-^{13}C]PC, examined previously[15], has been reanalyzed using k_{XS} and is shown in Figure 4B. At both sites the ^{13}C exhibits a small increase in R_1 due to the ^{13}C CSA (R_{CSA}, inset in Figure 4A) and a k_{XS} that is essentially the same for both ^{13}C-labeled sites. For P[1-^{13}C]OPC, the dashed line in Figure 4A shows the fit with $R_{D0}+k_{XS}+R_{CSA}$, where k_{XS} is estimated

from the fit in the inset. This approximation underestimates R_1 in the 10^7 to 10^8 rad s^{-1} region indicating that R_{D1} is still present, but its amplitude and correlation time are both reduced with respect to the *sn*-2 ^{13}C.
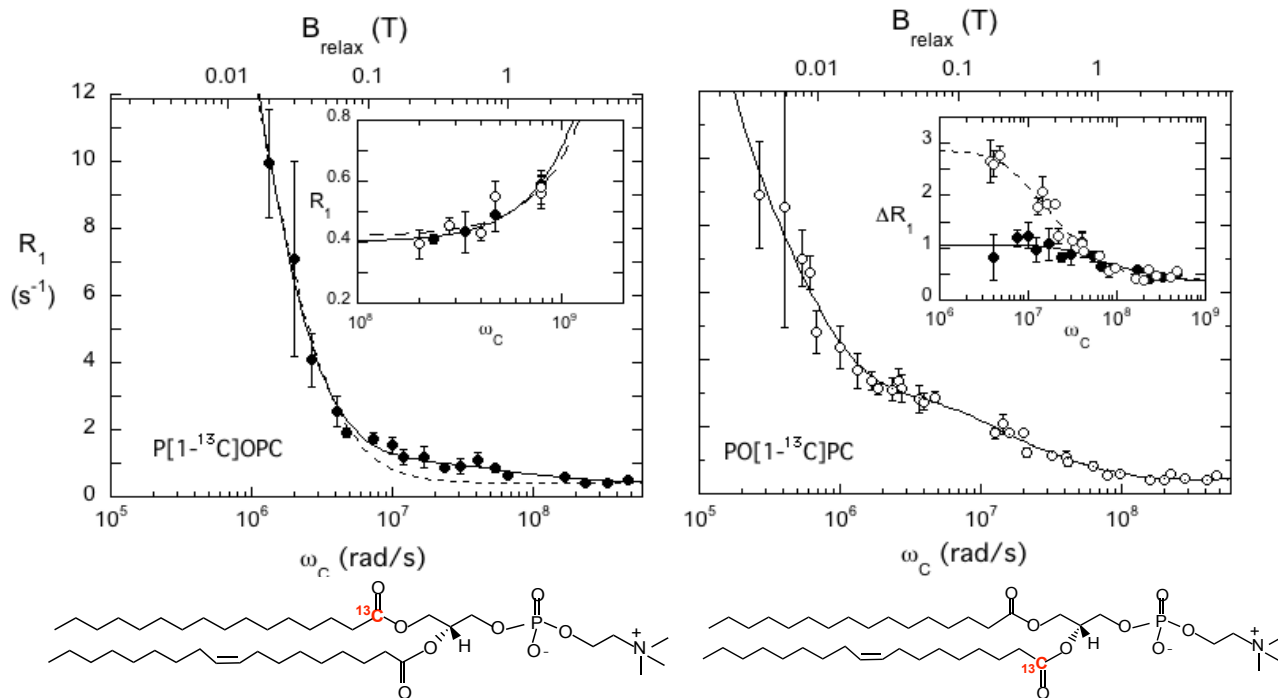

Figure 4. ^{13}C-labeled *sn*-1 and (left) and *sn*-2 (right) carbonyls of POPC in SUVs with equimolar unlabeled DOPMe. The highest field point (11.7 T), which shows an increase in R_1, is not shown allowing a fit to the sum of $R_{D0} + R_{D1} + k_{xs}$ as described in the Methods section. The dashed line for P[1-^{13}C]OPC is the best fit with a single dipolar term and constant, R_{D0}, and k_{xs}, the latter estimated as the average R_1 between 2 and 4 x10^8 rad s^{-1}. The inset in the P[1-^{13}C])PC panel shows the high frequency dependence of R_1 (fit to $k_{xs}+R_{CSA}$)., while the inset in the PO[1-^{13}C] panel shows the R_{D1} region for both labeled carbons, P[1-^{13}C]OPC (●) and PO[1-^{13}C]PC (○), after subtracting R_{D0} ($\Delta R_1 = R_1 - R_{D0}$). Below each graph is a structure of POPC showing the labeled ^{13}C.

The most striking difference for the two ^{13}C-labeled POPC samples is that as ω_C is decreased, the R_1 for P[1-^{13}C]OPC begins to increase significantly, well before the PO[1-^{13}C]PC R_1 does, consistent with a faster τ_{D0}. Also, magnetization of the *sn*-1 labeled ^{13}C decays so quickly below 2×10^6 rad s^{-1} that most of it is lost upon shuttling the sample back to the probe for readout. Fitting the limited data that we could acquire, we find that for P[1-^{13}C]OPC the $R_{D0}(0)$ is 3-fold higher than the value for the *sn*-2 ^{13}C, while the τ_{D0} value is ~ 0.7 μs, shorter than the ~ 1.5 μs value for PO[1-^{13}C]PC. The measured k_{XS} is the same for both ^{13}C sites. If cross-correlation relaxation is responsible for this NMRD, k_{XS} for P[1-^{13}C]OPC R_1 should be ~12-fold higher since $R_{CC} = R_{D0}(0)$ x k_{CSA}/τ_{D0}^2 in this frequency range. This discrepancy strongly supports identifying k_{XS} as $R_{D2}(0)$, at least for ^{13}C. Early studies of POPC acyl chain ^{13}C T_1 and NOE at four different Larmor frequencies found $\tau \sim 0.08$ ns for the α-^{13}CH$_2$.[28] The protons on that carbon likely dominate dipolar relaxation of the carbonyl ^{13}C label.

Since the sn-1 [13]C R_{D1} is small and partially overlapped by the large R_{D0}, we used τ_{D0} and $R_{D0}(0)$, from analyzing the low ω_C region separately, to subtract the portion of the [13]C R_1 caused by R_{D0}. For consistency this procedure was also applied to the sn-2 ^{13}C data (Figure 4B, inset). The ΔR_1 has contributions from R_{D1}, R_{CSA}, and $R_{D2}(0)$. Both τ_{D1} and $R_{D1}(0)$ are smaller for P[1-^{13}C]OPC, while the $\tau_{D1}/R_{D1}(0)$ ratio is similar for both ^{13}C-carbons (and smaller than for the [31]P – [1]H interaction) as expected since the α-CH$_2$ provide the major dipolar relaxation of each carbonyl [13]C. The shorter τ_{D1} is consistent with the sn-1 [1]H–C–[13]C undergoing more internal motion than the sn-2 chain ^{13}C, which is more constrained by the kink in its acyl chain.[29, 30] For P[1-^{13}C]OPC, the effective r_{CH} normalized to the two protons of the α-methylene group is 2.68 Å while it is 2.75Å for the sn-2. These values are closer to the r_{CH} values from the simulation, an average of 2.14 Å, than was observed for the [31]P. Again, if we introduce an order parameter, S_D^2 is ~ 0.24 for the two ^{13}C-C-[1]H$_2$ interactions.

SUVs of POPC with [1-^{13}C]oleic acid (3:1) make an interesting contrast to the POPC ^{13}C labels (Table 2 and Figure S4). The R_{D0} region has an amplitude similar to that of the sn-2 chain but a shorter τ_{D0}, 0.5 μs, comparable to the sn-1 [13]C (0.7 μs). The R_{D1} contribution is quite small even compared to that for the sn-1 [13]C. The oleate τ_{D1} is short and basically the same as that for the sn-1 [13]C (5 versus 4 ns) while $R_{D1}(0)$ and k_{XS} are half that for the sn-1 [13]C. Although the two POPC ^{13}C have different correlation times and amplitudes, $\tau_{D1}/R_{D1}(0)$ is the same. Since that ratio is two-fold larger for [1-^{13}C]oleate, it is likely that other nearby protons in the phospholipid molecule contribute to the sn-1 and sn-2 ^{13}C carbonyl R_1.

3. Dipolar relaxation of [1]H – a fast R_{D2} is observed

Shuttling ^{1}H field cycling was also carried out for small vesicles containing POPC/DOPMe (1:1). Three types of protons were monitored: the polar -N(CH$_3$)$_3$ group, the bulk methylenes (which sample the acyl chain protons of both phospholipids), and the acyl chain terminal methyl groups, ω-CH$_3$, from both POPC and DOPMe (Figure 5). The glycerol and choline methylene resonances were too overlapped to separate them cleanly as the relaxation field decreased below 0.1 T. There are two discrete NMRDs for the N-trimethyl group: R_{D0}, which begins to increase below 10^7 rad s^{-1} and has a correlation time of 0.3 μs (similar to values for the [31]P τ_{D0} ~0.5 μs) and a faster NMRD with a correlation time ~0.3 ns that we will label τ_{D2} since this is the region for R_{D2} for the two ^{13}C POPC probes. There is no obvious NMRD with a correlation time in the 10-20 ns range for these protons. The -N(CH$_3$)$_3$ protons are fairly isolated from other protons (4 bonds from the nearest choline methylene), and spin rotation of the methyl groups is likely the major relaxation mechanism.

Neither of the two acyl chain resonances exhibited a distinct low frequency NMRD comparable to R_{D0} (Figure 5 B and C). Relaxation for the bulk methylenes is characterized by two dipolar contributions: one with τ_{D1} = 21±8 ns (similar to the ^{31}P and [13]C τ_{D1}), and a second with τ_{D2} = 0.3±0.2 ns. Similarly, for the methyl groups at the end of the acyl chains, two dipolar NMRDs are observed: τ_{D1} = 14±4 ns and τ_{D2} = 0.2±0.1 ns. $R_{D1}(0)$ values are in the 2-5 s^{-1} range (Table 2). While the higher frequency NMRD is not well defined, it is clear that the sub-ns acyl chain and choline motions, chain librations and isomerizations and changes in dihedral angles, do relax the acyl chain and choline methyl protons on this time scale.
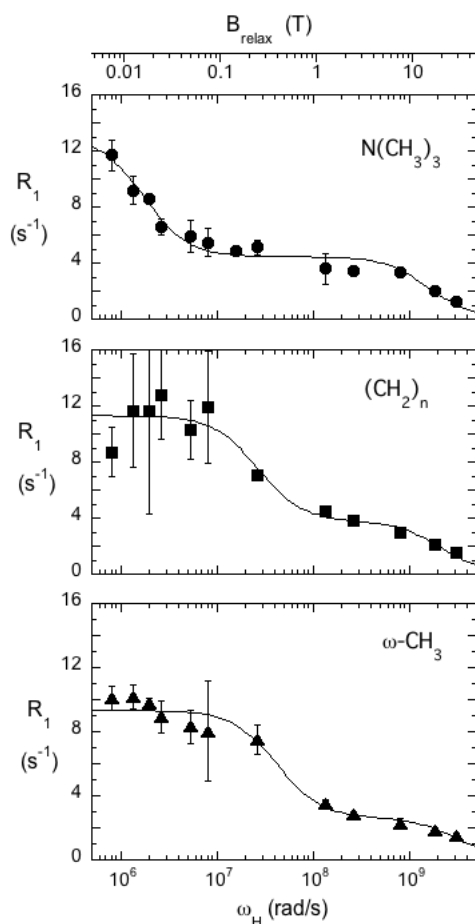
Figure 5. Dependence of POPC proton resonance R_1 on ω_H for POPC/DOPMe (1:1) SUVs: ●, $N(CH_3)_3$; ■, $(CH_2)_2$; ▲, ω-CH_3. The solid lines indicate the fit to each profile with two dipolar terms: $R_1 = R_{D0}$ (or R_{D1}) + R_{D2}.

DISCUSSION

An important advantage of using field cycling NMR relaxometry to characterize dynamics of phospholipids in bilayers is that different magnetic relaxation dispersions representing motions occurring on widely different time-scales are observed in the same experiment. High resolution shuttling relaxometry also provides the ability to compare NMRDs for ^{31}P, ^{13}C, and ^1H nuclei in the same molecule, thus providing a more complete picture of phospholipid dynamics and how different phospholipids in the same bilayer respond to the effect of additives.

τ_{D0} provides D_{lat} for different phospholipids in the same vesicle

For the small unilamellar vesicles we study, τ_{D0} should be ~2 μs if it reflects overall tumbling of the vesicles. However, for ^{31}P the extracted τ_{D0} is shorter (typically ~ 0.5 μs). A similar time-scale NMRD has been observed in fast-field cycling studies of vesicles, and has been attributed to

14

vesicle rotation and reorientation mediated by translational displacements.[7,8] This sensitivity of the ^{31}P R_{D0} to translational movements of phospholipids makes it useful for comparing this motion for different phospholipids in the same vesicle. As shown in Equation 6, the observed correlation time for a molecule on a curved surface is related to τ_{RD} (the vesicle rotational diffusion correlation time) and τ_{TD} (the surface translational diffusion correlation time),[31]

$$1/\tau_{D0} = 1/\tau_{RD} + 1/\tau_{TD} \qquad [6]$$

where $\tau_{RD} = 4\pi\eta\, r_v^3/3k_BT$, and $\tau_{TD} = r_v^2/6D_{TD}$ with r_v the average radius of the vesicles, η the solution viscosity, and D_{TD} the translational diffusion coefficient of the lipid.[7,8] For small POPC/DOPMe vesicles with an average radius of 125 Å, the τ_{TD} extracted from ^{31}P data for POPC is estimated as 0.88±0.11 µs and the $D_{TD} = (3.0\pm0.4)\mathrm{x}10^{-7}$ cm^2 s^{-1}. Since the DOPMe mixed with the POPC had basically the same τ_{D0}, that anionic phospholipid has the same D_{TD}. FFC experiments using larger vesicles of DMPC (540 Å radius)[8] yielded a D_{TD} of $0.8\mathrm{x}10^{-7}$ cm^2 s^{-1}.

A population of sonicated vesicles does not have a single size but a range of sizes. In the field cycling experiment, it is the low field R_{D0} NMRD that is sensitive to vesicle size. Errors in measuring R_1 are also largest at low field (<0.02 T). The population of larger vesicles will have R_{D0} shifted to lower fields and the experimentally extracted τ_{D0} is likely biased towards smaller vesicles. However, a particularly useful feature of R_{D0} is that it can be used to compare relative D_{TD} values for different phospholipid headgroups in the *same* vesicles under a variety of conditions.

As an example, the assignment of R_{D0} to vesicle rotation modulated by translation diffusion of phospholipids provides insights into the effect of a bacterial phosphatidylinositol-specific phospholipase C binding to POPC/DOPMe vesicles at various mole fractions (X_{PC}) of POPC where the ratio of phospholipid in the vesicle outer monolayer to protein was ~80:1, so that each vesicle will have many proteins on it (roughly 70-90 proteins per SUV for the phospholipid and proteins concentrations used).[32] The presence of POPC enhances the binding of the protein to DOPMe vesicles.[33] While both phospholipids can bind to the protein, they bind in different places.[34] The DOPMe binds in the active site while POPC molecules can form cation-π complexes with different protein Tyr residues.[35,36] Molecular dynamics simulations identify two long-lived PC cation / protein Tyr π complexes (and many other transient cation-π complexes between PC and Tyr residues with lower occupancies on a µs timescale) during simulations.[23,37] In the field cycling experiment with added protein, the DOPMe τ_{D0} decreased from ~ 0.5 µs at a mole fraction (X_{PC}) of 0.5 to 0.25 µs at $X_{PC} = 0.8$, a value comparable to what is measured for pure DOPMe vesicles. In contrast, the PC τ_{D0} was similar to that of the DOPMe at $X_{PC} = 0.5$ and increased slightly to 0.62 µs at $X_{PC} = 0.8$. In the PC-rich vesicles D_{TD} is $9.1\mathrm{x}10^{-7}$ cm^2 s^{-1} for the DOPMe and $2.9\mathrm{x}10^{-7}$ cm^2 s^{-1} for the POPC. Although the absolute value of D_{TD} may not be exact, it is clear that the translational movement of the DOPMe is enhanced about 3-fold compared to the POPC with a large amount of protein present. The added protein preferentially clusters the POPC molecules around it via multiple transient cation-π complexes. In turn, the DOPMe translational diffusion occurs in regions that have less POPC (and a higher proportion of DOPMe) and little accessible protein. Thus, ^{31}P R_{D0} NMRD is a useful tool for interrogating how proteins can selectively alter lipid translational diffusion, in this case monitoring demixing of two phospholipids by preferential interactions of the protein with one type of phospholipid.

R_{D1} affects acyl chain resonances as well as ^{31}P

A comparison of τ_{D1} extracted for phospholipid ^{13}C and ^1H as well as ^{31}P nuclei (Table 1) shows that *all* nuclear sites for phospholipids except the N-trimethyl protons exhibit an NMRD with a correlation time between 4 and 25 ns (average = 14±7). Thus, the molecular motion giving rise to this NMRD is not localized to the phosphate linkage but affects acyl chains as well. This would be expected for restricted motion about the long axis of the phospholipid. The τ_{D1} range is fairly large, which could arise from significant internal motion for some of these $^{31}P/^{13}C - {}^1H$ interactions. For example, the τ_{D1} for the *sn*-1 ^{13}C-labeled POPC carbonyl is significantly shorter than that for that of the *sn*-2 ^{13}C (4 versus 17 ns) consistent with more internal motion associated with the *sn*-1 carbonyl.

Previous ^{31}P and ^{13}C NMR studies have shown that cholesterol does little to the PC ^{31}P conformation[38] or order parameters for glycerol and choline moieties[39]. ^{31}P and ^{13}C field cycling experiments for PC molecules show that τ_{D1} is increased by inclusion of cholesterol, typically about 3-fold.[15, 20] If wobble of a roughly cylindrical phospholipid molecule is responsible for the ^{31}P R_{D1}, an increase in τ_{D1} would be expected when the rigid steroidal rings are in the bilayer. Consistent with this, MD simulations of different phospholipid bilayers with cholesterol added show an increase in the lipid wobble time comparable to what is observed with field cycling.[40]

We can extract more information from looking at how cholesterol affects $R_{D1}(0)$ as well as τ_{D1} (Figure S5) Analysis of previous data for DOPMe/POPC/cholesterol (1:1:1) at 40°C using k_{xs} yields τ_{D1} values for both phospholipids around 30 ns, roughly 3-fold higher than in the absence of cholesterol. However, $R_{D1}(0)$ in the presence of the sterol is similar to the value the phospholipids in its absence.[20] With cholesterol, $\tau_{D1}/R_{D1}(0)$ is 4 to 5x10^{-8} s^2, a value comparable to that for d$_{75}$-DPPC where the choline protons have been deuterated. If the choline methylene contribution to ^{31}P relaxation now has a shorter correlation time than the glycerol moiety, there would be a separate NMRD at higher fields. However, this would have a lower magnitude and likely to be difficult to distinguish from a high field tail of the glycerol ^{31}P- O-CH$_2$- interaction and the k_{xs} contribution. If one examines the dependence of ΔR_1 (subtracting R_{D0}) on the relaxation field, the region between 0.5 and 2-3 T is not well fit when using $R_{D1}+k_{xs}+k_{CSA}$ (Figure S5B) and the higher than expected R_1 is likely for the faster choline – ^{31}P interaction. Thus, the presence of cholesterol retards the wobble motion of the phospholipid but has little effect on the choline moiety. Thus, analysis of the ^{31}P R_{D1} NMRD indicates cholesterol uncouples the choline motion from the glycerol backbone on the tens of ns time-scale.

A third dipolar NMRD is responsible for the ^{31}P k_{xs} and improves the estimation of θ_{PH}

For both the ^{31}P and ^{13}C, two dipolar and one CSA NMRD are not adequate to describe the dependence of R_1 on Larmor frequency. There is clearly 'excess' R_1 between R_{D1} and R_{CSA} which we have now treated as a constant, k_{xs}, in the analysis of the relaxation profiles. The two most likely interactions for this higher than expected R_1 are (1) a dipolar/CSA cross-relaxation, or (2) a faster high frequency dipolar interaction where $\omega^2\tau^2 << 1$ in this region. For the ^{13}C-carbonyls, k_{xs} cannot arise from cross-correlation relaxation because k_{xs} is the same for both carbonyls. Since a fast τ_{D2} must account for k_{xs} for the ^{13}C carbonyls, and 0.1-0.3 ns τ_{D2} values are observed for all three POPC ^1H probes, it is likely that a similar high frequency dipolar interaction is also

responsible for the ^{31}P k_{xs}. The α-methylene ^{13}C–H protons are closest to the ^{13}C carbonyl, and we can use the correlation value for their fast motion, 0.08 ns, as an approximation for τ_{D2}.[28] After subtraction of R_{D0} and R_{D1} (using the parameters from Table 1), the resultant ΔR_1 is equal to the sum $R_{D2} + R_{CSA}$. The fit with 0.08 ns as τ_{D2} yields $R_{D2}(0) = 0.38\pm0.03$ s^{-1} and $k_{CSA} = (3.7\pm1.3)$x10^{-19} (Figure S6). This added dipolar term also explains why the apparent ^{13}C R_{CSA} is so small for the carbonyl. $R_{D2}(0)$ masks the CSA relaxation; significantly higher fields would be needed to analyze R_{CSA} accurately (Figure S6B).

The POPC ^{31}P R_1 data shown in Figure 1 has a more defined CSA dispersion. We can add a third dipolar interaction, R_{D2}, and fit the data for $\omega_P > 1$x10^7 rad s^{-1} (there is negligible R_{D0} contribution above that frequency) to $R_{D1}+R_{D2}+R_{CSA}$. If we assume $R_{D2}(0) = 0.4$ s^{-1} (the k_{xs} value), the least-square fit yields $\tau_{D1} = 10\pm2$ ns, $R_{D1}(0) = 0.75\pm0.07$ s^{-1} (both similar to the analysis shown in Table 1), and $\tau_{D2} = 0.24\pm0.15$ ns. Although τ_{D2} is not well-determined, it is in the range of the values seen for the ^{1}H probes and also agrees with a correlation time for fast motion extracted for ^{31}P of DMPC (0.4-0.7 ns).[4] The contributions of the individual relaxation components are shown in Figure 6A. The same analysis for DOPA in borate (inset of Figure 3) yields $\tau_{D1} = 9\pm2$ ns, $R_{D1}(0) = 0.58\pm0.06$ s^{-1}, $\tau_{D2} = 0.3\pm0.2$ ns, and $R_{D2}(0) = 0.25\pm0.02$ s^{-1} (Figure 6B). The decreased $R_{D2}(0)$ compared to POPC is consistent with the lack of a polar head group esterified to the DOPA.

The ratio of the area of the R_{D0} NMRD, A_{D0}, compared to the sum of all the areas of the dipolar NMRDs (Equation 7) can be used to estimate an average angle of the ^{31}P-to-H vector with respect to the bilayer normal.[13]

$$A_{D0}/\Sigma\ A_{Di} = ¼\ (3\cos^2\theta_{PH} - 1)^2 \qquad\qquad [7]$$

For this analysis to give a reasonable value for θ_{PH} *all* the dipolar NMRDs for a phospholipid in a vesicle must be summed. We can compare the value obtained from the field cycling experiment with what is observed in analyzing an MD simulation of a DMPC bilayer[22]. From the simulation, θ_{PH} is $50\pm1°$ for the glycerol P – H vector and $90\pm2°$ for the choline P – H vector (Table 2).

For d$_3$-DOPMe, only the glycerol -CH$_2$O- contributes to ^{31}P dipolar relaxation. Using just R_{D0} and R_{D1} parameters, we find the possible magnitudes for θ_{PH} are $40°$ and $74°$. Adding R_{D2} yields angles of $49°$ or $61°$. Clearly, the value of $49°$ agrees well with the DMPC simulation. If we do the same dipolar area analysis for POPC, we find the θ_{PH} magnitude is predicted to be $46°$ or $64°$ – very close to the value for the glycerol methylene to phosphorus vector. One might expect the choline ^{31}P-O-C-^{1}H$_2$ interaction to affect the average θ_{PH}. However, faster motions of the choline could randomize that vector with respect to the bilayer normal over 1-2 μs. In contrast, the geometry of the glycerol ^{31}P-O-C-^{1}H vector with respect to the bilayer surface is much more constrained. On the μs timescale, the POPC θ_{PH} only reflects the glycerol ^{31}P – ^{1}H orientation consistent with the polar headgroup motion significantly faster than the rest of the molecule.
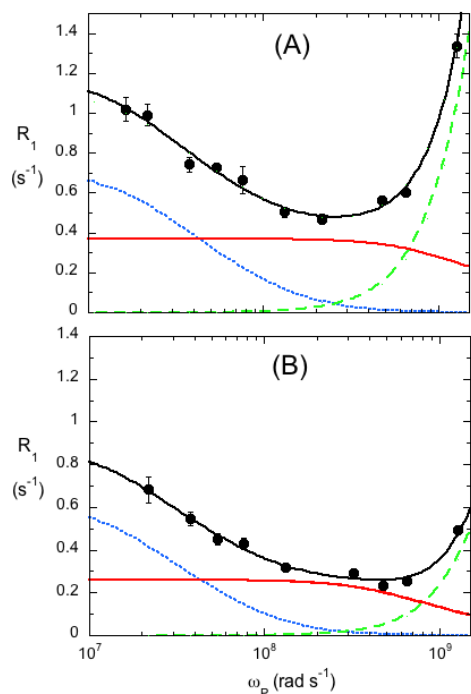
Figure 6. Analysis of the R_1 dependence ($\omega_P > 10^7$ rad s^{-1}) on ω_P as $R_1 = R_{D1} + R_{D2} + R_{CSA}$ for (A) POPC and (B) DOPA (in borate buffer). Individual relaxation contributions include R_{D1} (blue), R_{D2} (red) and R_{CSA} (green).

Prospects for heteronuclear shuttle field cycling

With the nuclear magnetic resonance dispersions observed in high resolution ^{31}P and ^{13}C field cycling now attributed to specific motions, it should be straightforward to interpret changes for different phospholipids in the same vesicle, as long as their chemical shifts are separable. One of the real advantages of this variant of field cycling is that multiple NMRDs are detected in the same experiment and, depending on the motion responsible, are sensitive to different perturbants, including ones that partition into the bilayer (e.g., cholesterol and peripheral proteins) but also soluble molecules that can bind to a specific phospholipid (i.e., the Tris cation binding to phosphatidic acid). NMRDs comparable to R_{D0} and R_{D1} as well as the 'excess' R_1 attributed to R_{D2} are also observed for phospholipids in micelles[41] and nanodiscs (S. Jayaraman, O. Gursky, and M. F. Roberts, unpublished results). Thus, heteronuclear field cycling from 0.003 to 11.7 T provides measures of translational diffusion of different phospholipids in a particular aggregate, molecular wobbling and how these motions are affected by temperature, non-phospholipid additives, etc. Very fast local motions can also be quantified using the same set of experimental data. Recent advances in field cycling systems should extend the methodology to many more membrane related systems. There is now a shuttler for standard bore magnets with a cryo-probe[42] and a shuttling system compatible with magic-angle spinning[43]. The latter allows studies on larger bilayer systems and was used to examine a photosynthetic reaction center. For ^{31}P in particular, this may open up a wide variety of experiments focusing on motional behavior of phospholipid polar headgroups.

CONCLUSIONS

1. Polar headgroup protons as well as glycerol protons contribute to the dipolar ^{31}P R_1. For phosphatidic acid (A), without a polar ester, cationic organic buffers can form transient complexes with the PA that contribute to significant dipolar relaxation.

2. Identification of the lowest field NMRD for these vesicles as resulting from overall vesicle tumbling that includes translational diffusion of phospholipids provides a way of estimating lateral diffusion constants for different phospholipids in the same bilayer. The usefulness of this is illustrated with a peripheral membrane protein that forms transient PC cation – tyrosine-π phosphatidylcholine complexes. An anionic phospholipid in a PC-rich bilayer exhibits a three-fold increase in translational diffusion compared to PC consistent with the formation of PC/protein clusters that tend to exclude the anionic phospholipid.

3. ^{13}C-labeled carbonyls and acyl chain ^{1}H resonances, as well as ^{31}P exhibit a dipolar NMRD with a 10-20 ns correlation time consistent with wobble of the phospholipid in a cone. The inclusion of cholesterol impedes this motion and the significantly longer ^{31}P – ^{1}H distance that is derived from $\tau_{D1}/R_{D1}(0)$ implies that the motion of the choline is uncoupled from the decreased wobble motion of the phospholipid molecule in the presence of the sterol.

4. 'Excess' ^{31}P and ^{13}C R_1 around 2-5x10^7 rad s^{-1} is assigned to a third dipolar interaction with a correlation time < 0.5 ns. The ratio of the μs NMRD compared to the summed area of all three dispersions provides an estimate of the average of the ^{31}P – ^{1}H angle with respect to the bilayer normal. POPC, DOPMe, and d$_3$-DOPMe yield essentially the same angle indicating the choline or methanol is sufficiently mobile so that the ^{31}P – ^{1}H vector for the polar head group does not have a preferred orientation on a μs timescale.

SUPPORTING INFORMATION

Structures (and where relevant synthesis) for isotopically phospholipids used; Larmor frequency dependence of R_1 for the choline ^{31}P-O-C-^{1}H interaction; effect of buffer on the ^{31}P chemical shift of dioleoylphosphatidic acid in small unilamellar vesicles with POPC. ^{13}C; field cycling profiles for [1-^{13}C]oleate in unlabeled POPC vesicles; **^{31}P** field cycling profiles for DOPMe/POPC/cholesterol; extraction of R_{D2} parameters for the *sn*-2 ^{13}C-labeled POPC.

AUTHOR INFORMATION

Corresponding author: mary.roberts@bc.edu

PRESENT ADDRESSES:

V. N. Sivanandam, CICbioGUNE, Parque Tecnologico de Bizakaia, Ed. 800, Derio, 48160, Spain; H. M. Khan, Centre for Molecular Simulation, Department of Biological Sciences, University of Calgary, Calgary, Alberta, Canada

NOTES: The authors declare no competing financial interest.

ACKNOWLEDGMENT

ABBREVIATIONS

CSA, chemical shift anisotropy; DMPC, dimyristoylphosphatidylcholine; DOPA, dioleoyl-phosphatidic acid; DOPMe, dioleoylphosphatidylmethanol; DPPC, dipalmitoylphosphatidyl-choline; FFC, fast field cycling; LUV, large unilamellar vesicle; NMRD nuclear magnetic relaxation dispersion; PA, phosphatidic acid; PC, phosphatidylcholine; POPC, 1-palmitoyl-2-oleoyl-PC; R_1, spin-lattice relaxation rate; SUV, small unilamellar vesicle

REFERENCES

(1)   Gupta, S.; De Mel, J.U.; Schneider, G.J. Dynamics of Lipososmes in the Fluid Phase. *Curr. Op. Coll. Int. Sci.* **2019**, *42*, 121-136.

(2)   Flores-Romero, H.; Ros, U.; García-Sáez, A. J. A Lipid Perspective on Regulated Cell Death. *Int. Rev. Cell. Mol. Biol.* **2020**, *351*,197-236.

(3)   Katan, M; Cockcroft, S. Phospholipase C Families: Common Themes and Versatility in Physiology and Pathology. *Prog. Lipid Res.*, **2020**, *80*, 101065.

(4)   Dufourc, E.J.; Mayer, C.; Stohrer, J.; Althoff, G.; Kothe, G. Dynamics of Phosphate Head Groups in Biomembranes. Comprehensive Analysis Using Phosphorus-31 Nuclear Magnetic Resonance Lineshape and Relaxation Time Measurements. *Biophys. J.* **1992**, *61*, 42-57.

(5)   Roberts, M. F.; Redfield, A. G. High Resolution [31]P Field Cycling As a Probe of Phospholipid Dynamics. *J. Amer. Chem. Soc*. **2004**, *126*, 13765-13777.

(6)   *Field-Cycling NMR Relaxometry. Instrumentation, Model Theories and Application*s (R. Kimmich, editor), Royal Society of Chemistry, *New Developments in NMR No. 18*, **2019**.

(7)   Meledandri, C. J.; Perlo, J.; Farrher, E.; Brougham, D. F.; Anoardo, E. (2009) Interpretation of Molecular Dynamics on Different Time Scales in Unilamellar Vesicles Using Field-Cycling NMR Relaxometry. *J. Phys. Chem. B.*, **2009**, *113*, 15532-15540.

(8)   Perlo, J.; Meledandri, C. J.; Anoardo, E.; Brougham, D.F. (2011) Temperature and Size-Dependence of Membrane Molecular Dynamics in Unilamellar Vesicles by Fast Field-Cycling NMR Relaxometry. *J. Phys. Chem. B* **2011**, *115*, 3444-3451.

(9)   Wagner, S.; Denisen, T. R. J.; Rayner, T.; Bryant, R. G. High Resolution Magnetic Dispersion Measurements of Solute Spin Probes Using a Dual Magnet System. *J. Magn. Reson.* **1999**, *140*, 172–178.

(10)   Victor, K.; Kavolius, V.; Bryant, R. G. Magnetic Relaxation Dispersion Probe. *J. Magn. Reson.* **2004**, *171*, 253–257.

(11)   Victor, K.; Van-Quynh, A.; Bryant, R. G. High Frequency Dynamics in Hemoglobin Measured by Magnetic Relaxation Dispersion. *Biophys. J.* **2005**, *88*, 443-454.

(12)   Redfield, A. G. High Resolution NMR Field-Cycling Device for Full-Range Relaxation and Structural Studies of Biopolymers on a Shared Instrument. *J. Biomol. NMR* **2012**, *52*, 159-177.

(13)   Roberts, M. F.; Redfield, A. G. Phospholipid Bilayer Surface Configuration Probed Quantitatively by ^{31}P Field-Cycling NMR. *Proc. Natl. Acad. Sci. U.S.A.* **2004**, *101*, 17066-17071.

(14)   Klauda, J. B.; Roberts, M. F.; Redfield, A. G.; Brooks, B. R.; Pastor, R. W. (2008) Rotation of Lipids in Membranes: MD Simulation, ^{31}P Spin-Lattice Relaxation, and Rigid-Body Dynamics. *Biophys. J.* **2008**, *94*, 3074-3083.

(15)   Sivanandam, V. N.; Cai, J.; Redfield, A. G.; Roberts, M.F. Phosphatidylcholine "Wobble" in Vesicles Assessed by High-Resolution ^{13}C Field Cycling NMR Spectroscopy. *J. Am. Chem. Soc.* **2009**, *131*, 3420-3421.

(16)   Pu, M.; Roberts, M. F.; Gershenson, A. Fluorescence Correlation Spectroscopy of Phosphatidylinositol-Specific Phospholipase C Monitors the Interplay of Substrate and Activator Lipid Binding. *Biochemistry* **2009**, *48*, 6835-6845.

(17)   Roberts, M. F.; Cui, Q.; Turner, C. J.; Case, D. A.; Redfield, A. G. High-Resolution Field-Cycling Studies of a DNA Octamer as a Probe of Phosphodiester Dynamics and Comparison with Computer Simulation. *Biochemistry* **2004**, *43*, 3637-3650.

(18)   Guard-Friar, D.; Chen, C.; Hwei, C.; Engle, A.S. Deuterium Isotope Effect on the Stability of Molecules: Phospholipids. *J. Phys. Chem.* **1985**, *89,* 1810-1813.

(19)   Kumar, A.; Grace, R. C. R.; Madhu, P. K. Cross-Correlations in NMR. *Progr. Nucl. Magn. Reson. Spectrosc.* **2000**, *37*, 191-319.

(20)   Roberts, M. F.; Mohanty, U.; Redfield, A. G. Phospholipid Reorientation at the Lipid/Water Interface Measured by High Resolution Field Cycling ^{31}P NMR Spectroscopy. *Biophys. J.* **2009**, *97*, 132-141.

(21)   Wu, W.; Noble, D. L.; Owers-Bradley, J. R.; Horsewill, A. J. A ^{13}C Field-Cycling NMR Relaxometry Investigation of Proton Tunneling in the Hydrogen Bond: Dynamic Isotope Effects,

the Influence of Heteronuclear Interactions, and Coupled Relaxation. *J. Mag. Res.* **2005**, *175*, 210-221.

(22)   Grauffel, C.; Yang, B.; He, B.; Roberts, M.F.; Gershenson, A.; Reuter, N. Cation-π Interactions as Lipid-Specific Anchors for Phosphatidylinositol-Specific Phospholipase C. *J. Am. Chem. Soc.* **2013**, *135*, 5740-5750.

(23)   Klauda, J. B.; Venable, R. M.; Freites, J. A.; O'Connor, J. W.; Tobias, D. J.; Mondragon-Ramirez, C.; Vorobyov, I.; MacKerell, A. D., Jr.; Pastor, R. W. Update of the CHARMM All-Atom Additive Force Field for Lipids: Validation on Six Lipid Types. *J. Phys. Chem. B* **2010**, 114, 7830–7843.

(24)   Guixà-González, R.; Rodríguez-Espigares, I.; Ramírez-Anguita, J.M.; Carrió-Gaspar, P.; Martinez-Seara, H.; Giorgino, T.; Selen, J. MEMBPLUGIN: Studying Membrane Complexity in VMD. *Bioinformatics* 2014, *30*, 1478-1480.

(25)   Humphrey, W.; Dalke, A.; Schulten, K. VMD: Visual Molecular Dynamics. *J. Molec. Graphics* **1996**, *14*, 33−38.

(26)   Kulig, W.; Korolainen, H.; Zatorska, M.; Kwolek, U.; Wydro, P.; Kepczynski, M.; Rog, T. Complex Behavior of Phosphatidylcholine – Phosphatidic Acid Bilayers and Monolayers: Effect of Acyl Chain Unsaturation. *Langmuir* **2019**, *35*, 5944-5956.

(27)   Swairjo, M. A.; Seaton, B. A.; Roberts, M. F. Effect of Vesicle Composition and Curvature on the Dissociation of Phosphatidic Acid in Small Unilamellar Vesicles – a ^{31}P NMR Study. *Biochim. Biophys. Acta* **1994**, *1191*, 354-361

(28)   Lepore, L. S.; Ellena, J. F.; Cafiso, D. S. Comparison of the Lipid Acyl Chain Dynamics Between Small and Large Unilamellar Vesicles. *Biophys. J.* **1992**, *61*, 767-775.

(29)   Hong, M.; Schmidt-Rohr, K.; Nanz, D. Study of Phospholipid Structure by ^{1}H, ^{13}C, and [31]P Dipolar Couplings from Two-Dimensional NMR. *Biophys. J.* **1995**, *69*, 1939-1950.

(30)   Hong, M.; Schmidt-Rohr, K.; Zimmerman, H. Conformational Constraints on the Headgroup and *sn*-2 Chain of Bilayer DMPC from NMR Dipolar Couplings. *Biochemistry* **1996**, *35*, 8335.

(31)   Halle, B. Theory of Spin Relaxation by Diffusion on Curved Surfaces. *J. Chem. Phys.* **1991**, *94*, 3150-3168.

(32)   Pu, M.; Fang, X.; Gershenson, A.; Redfield, A. G.; Roberts, M. F. Correlation of Vesicle Binding and Phospholipid Dynamics with Phospholipase C Activity: Insights into Phosphatidylcholine Activation and Surface Dilution Inhibition. *J. Biol. Chem.* **2009**, *284*, 16099-16107.

(33)   Yang, B.; Pu, M.; Khan, H.; Friedman, L.; Reuter, N.; Roberts, M.F.; Gershenson, A. Quantifying Transient Interactions Between *Bacillus* Phosphatidylinositol-specific Phospholipase C and Phosphatidylcholine-rich Vesicles. J. *Am. Chem. Soc*. **2015**, *137*, 14-17.

(34)   Pu, M.; Orr, A.; Redfield, A. G.; Roberts, M. F. Defining Specific Lipid Binding Sites for a Membrane Protein *in situ* Using Subtesla Field-Cycling. *J. Biol. Chem.* **2010**, *285*, 26916-26922.

(35)   Cheng, J.; Goldstein, R.; Gershenson, A.; Stec, B.; Roberts, M.F. The Cation-π Box is a Specific Phosphatidylcholine Membrane Targeting Motif. *J. Biol. Chem.* **2013**, *288*, 14863-14873.

(36)   He, T.; Gershenson, A.; Eyles, S. J.; Lee, Y.-J.; Liu, W. R.; Wanf, J.; Gao, J.; Roberts, M. F. Fluorinated Aromatic Amino Acids Distinguish Cation-π Interactions from Membrane Insertion. *J, Biol, Chem.* **2015**, *290*, 19334-19342.

(37)   Waheed, Q.; Khan, H. M.; He, T.; Roberts, M. F.; Gershenson, A.; Reuter, N. Interfacial Aromatics Mediating Cation-π Interactions with Choline-Containing Lipids Can Contribute as Much to Peripheral Protein Affinity for Membranes as Aromatics Inserted Below the Phosphates. *J. Phys. Chem. Lett.*, **2019**, *10*, 3972-3977.

(38)   Brown. M. F.; Seelig, J. (1978) Influence of Cholesterol on the Polar Region of Phosphatidylcholine and Phosphatidylethanolamine Bilayers. *Biochemistry*, **1978**, *17*, 381-384.

(39)   Ferreira, T. M.; Coreta-Gomes, F.; Ollila, O. H.; Moreno, M. J.; Vaz, W. L.; Topgaard, D. Cholesterol and POPC Segmental Order Parameters in Lipid Membranes: Solid State ^{1}H-^{13}C NMR and MD Simulation Studies. *Phys. Chem. Chem. Phys.*, **2013**, *15*, 1976-89.

(40)   Boughter, C. T.; Monje-Galvan, V.; Im, W.; Klauda, J. B. Influence of cholesterol on phospholipid bilayer structure and dynamics. *J. Phys. Chem. B*, **2016**, *120*, 11761-11772.

(41)   Roberts, M. F. High-Resolution Applications of Shuttle Field-Cycling NMR. In *Field-cycling NMR Relaxometry. Instrumentation, Model Theories and Applications.* New Developments in NMR, **2018**, *18*, 385-404.

(42)   Chou, C.-Y.; Chu, M.; Chang, C.-F.; Yu, T.; Huang, T.; Sakellariou, D. High Sensitivity High-Resolution Full Range Relaxometry Using a Fast Mechanical Sample Shuttling Device and a Cryo-probe. *J. Biomol. NMR*, **2016**, *66*, 187-194.

(43)   Gräsing, D.; Bielytskyi, P.; Céspedes-Camacho, I.F.; Alia, A.; Marquardsen, T.; Engelke, F.; Matysik, J. Field-Cycling NMR with High-Resolution Detection Under Magic-Angle Spinning: Determination of Field-Window for Nuclear Hyperpolarization in a Photosynthetic Reaction Center. *Sci. Rep*. **2017**, *7*, 12111.

TOC
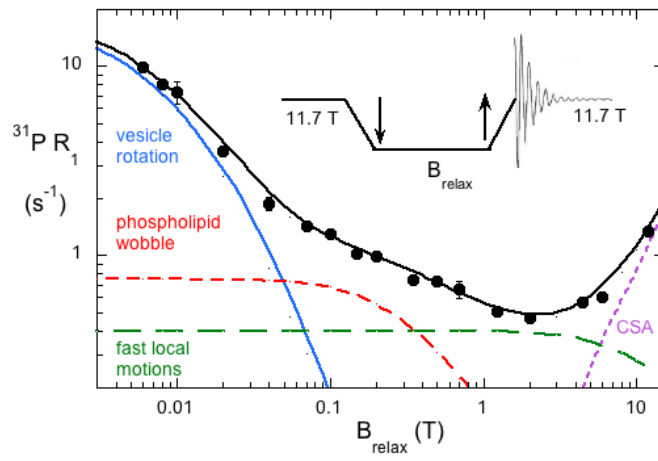
SUPPORTING INFORMATION

1. **Figure S1**. Isotopically labeled phospholipids used and schematics of phospholipid motions that are detected in ^{31}P field cycling experiments on vesicles

2. **Synthesis of ^{13}C-labeled carbonyls in POPC**

3. **Figure S2.** Larmor frequency dependence of R_1 for the choline ^{31}P-O-C-^{1}H interaction

4. **Figure S3.** Effect of buffer on the ^{31}P chemical shift of dioleoylphosphatidic acid in small unilamellar vesicles (SUVs) with POPC.

5. **Figure S4**. ^{13}C shuttling field cycling profiles for [1-^{13}C]oleate in unlabeled POPC vesicles compared to the *sn*-1 and *sn*-2 carbonyls of POPC.

6. **Figure S5.** ^{31}P field cycling profiles for DOPMe/POPC/cholesterol (1:1:1) SUVs at 40ºC.

7. **Figure S6.** Extracting R_{D2} parameters for the *sn*-2 ^{13}C-labeled POPC.

Figure S1. Isotopically labeled phospholipids used and schematics of phospholipid motions that are detected in ^{31}P field cycling experiments on vesicles. The d$_{75}$-DPPC structure was taken from https://avantilipids.com/product/860358. The other structures are from the Avanti web site but modified to show stable isotope position. Also shown are diagrams of the three motions giving rise to ^{31}P NMRDs: R$_{D0}$ reflects overall vesicle rotation that also includes lateral diffusion of the phospholipids; R$_{D1}$ reflects wobbling of the phospholipid long axis in a cone.
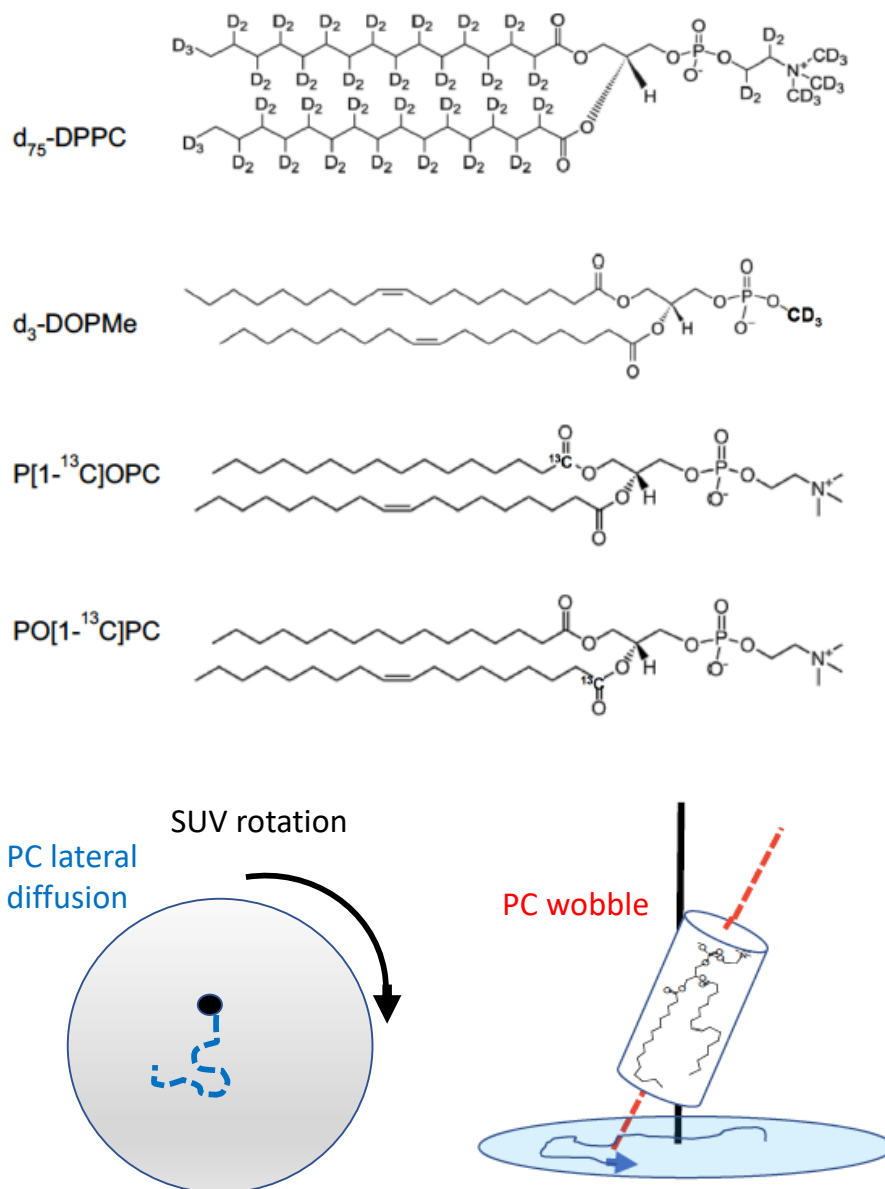
Synthesis of ¹³C-labeled carbonyls in POPC molecules

The synthesis of *sn*-2 ¹³C- carbonyl labeled POPC, PO[1-¹³C]PC, from 1-palmitoyl-PC using N,N'- dicyclohexylcarbodiimide activated [1-¹³C]oleic acid (Cambridge Isotopes) was previously reported.[1] Under some conditions, there may be migration of the acyl chain to form 2-lyso-PC which will subsequently be acylated with 1-¹³C]oleic acid. The two carbonyl carbons of POPC (and other PC species) are separable in the ¹³C spectrum when the phospholipid is solubilized in CD_3OD, and relative ¹³C intensities can be used to analyze for any isomerization of the lyso-1-palmitoyl-PC to 2-palmitoyl-PC and subsequent reacylation to O[1-¹³C]PPC. We could not detect a distinct peak for that side product (with the phospholipid dispersed in CD_3OD) and set a conservative upper limit for any OPPC generated at 10%. As seen in the Results, although the *sn*-1 ¹³C-labeled contaminant, would presumably exhibit much higher R_1 values at very low fields than the major compound, below 10^6 rad s^{-1} that small amount would decay very quickly and would not appreciably contribute to the PO[1-¹³C]PC profile at low fields. The contribution to the R_{D1} NMRD would also be small since the *sn*-1 ¹³C NMRD has a roughly 2-fold lower amplitude than does the *sn*-2 ¹³C label.

POPC with the *sn-1* carbonyl labeled, P[1-¹³C]OPC, was synthesized in three steps. (i) Acylation of *sn*-glycerol-3-phosphocholine with N,N'-dicyclohexylcarbodiimide activated [1-¹³C]-palmitic acid in an anhydrous $CHCl_3$ / 4-(dimethylamino)pyridine mixture generated DPPC with both chains containing ¹³C labeled carbonyls. This material was purified via silica gel chromatography. (ii) Treatment of ¹³C-labeled DPPC (solubilized in diethyl ether/methanol/water (9:1:0.2 v/v/v) with bee venom phospholipase A_2 (Sigma-Aldrich Chemical Co.), introduced as a 1 mg/ml solution in 100 mM Tris, pH 7.5, with and 7 mM Ca^{2+}, generated the 1-[1-¹³C]palmitoyl-PC lyso-phospholipid. After the removal of the organic solvent, the reaction mixture was washed with diethyl ether, lyophilized, and then dissolved in ~10 ml $CHCl_3/CH_3OH$ (2:1, v/v) and centrifuged at 4,000 rpm for 20 min to remove the precipitate. (iii) The *sn*-1 ¹³C-labeled lyso-phospholipid was then reacylated with N,N'-dicyclohexylcarbodiimide activated unlabeled oleic acid. The final product, P[1-¹³C]OPC, was purified by elution through a silica gel column and incorporation of the ¹³C was confirmed by ¹H, ³¹P and ¹³C NMR and mass spectrometry. Analysis of the ¹³C spectrum of the product PC in CD_3OD indicated a small amount (~8%) of ¹³C at the sn-2 position. This could reflect a small amount of remaining DPPC with both carbonyls labeled, or reacylation of the isomerization product 2-[1-¹³C]palmitoyl-PC.

[1] Sivanandam, V. N.; Cai, J.; Redfield, A. G.; Roberts, M.F. *J. Am. Chem. Soc.* **2009**, *131*, 3420-3421.

Figure S2. Larmor frequency dependence of R_1 for the choline ^{31}P-O-C-^1H interaction.

choline -C^{1}H$_2$-O-^{31}P- contribution
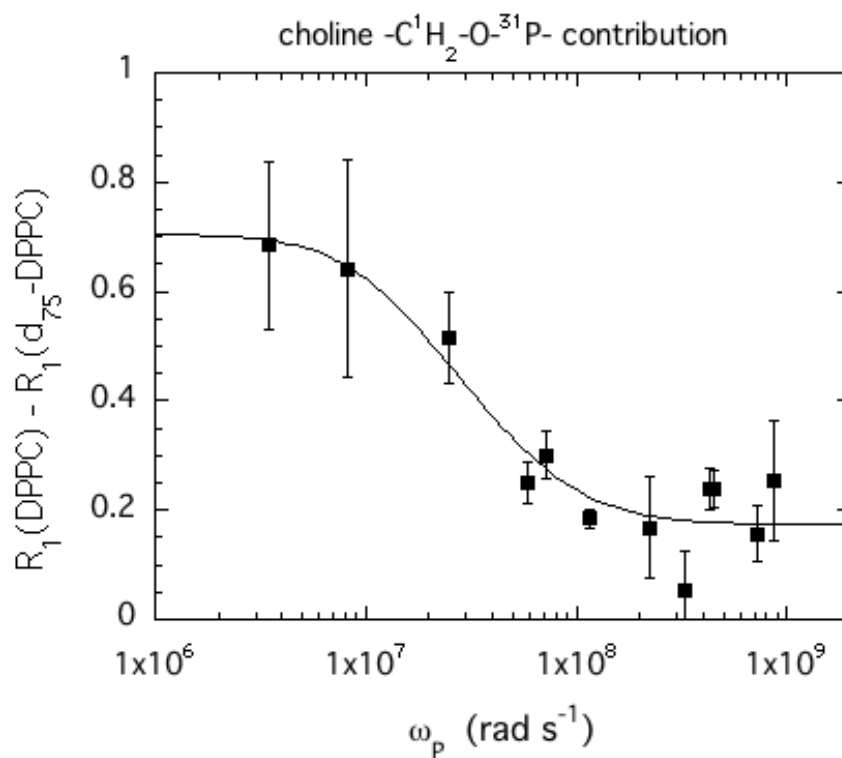
R_1 values for DPPC minus the contribution from d$_{75}$-DPPC (estimated by the best fit shown in Figure 3B) were fit with $R_1 = R_{D1}+k_{xs}$ (solid line). Extracted parameters for the choline –CH$_2$O-P contribution include: $\tau_{D1} = 16\pm5$ ns, $R_{D1}(0) = 0.53\pm0.06$ s^{-1}, and $k_{xs} = 0.17\pm0.03$ s^{-1}

Figure S3. Effect of buffer on the ^{31}P chemical shift (and hence the pK_{a2}) of 5 mM dioleoylphosphatidic acid (DOPA) in small unilamellar vesicles (SUVs) with 10 mM POPC.
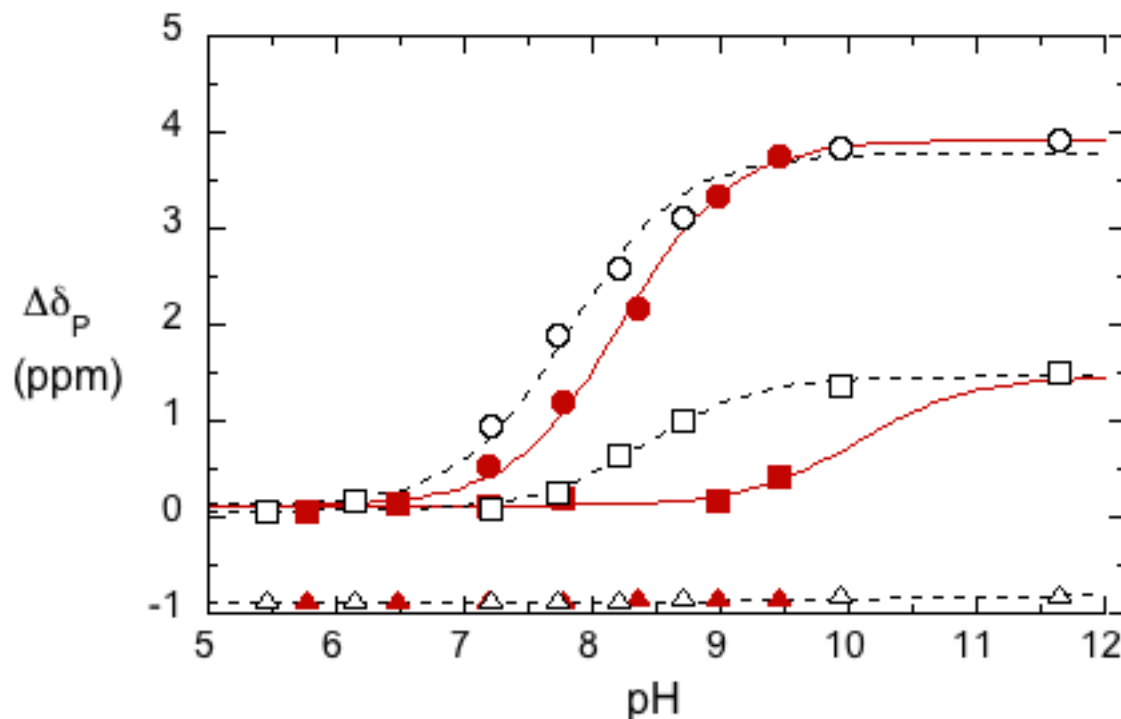

The circles, represent DOPA in the outer monolayer, squares represent DOPA in the inner monolayer, and triangles are for POPC. Empty symbols are for the vesicles in 50 mM Tris HCl and filled symbols are for the SUVs in 50 mM sodium borate. For the inner monolayer DOPA in sodium borate, the curve shown assumes the final deprotonated chemical shift will be the same as that for the same resonance in Tris. SUVs also contained 1 mM EDTA, and 1 mM glycerophosphocholine, the latter added as a chemical shift standard (its chemical shift is invariant between pH 5 and 12). Spectra were acquired as a function of pH on a Varian VNMRS 600 MHz spectrometer. The pH of the solution, measured before and after obtaining a spectrum, was adjusted by titrating with 6 N HCl or 10 N NaOH (to minimize volume change), followed by resonication prior to measurement.

Figure S4. ^{13}C shuttling field cycling profiles for [1-^{13}C]oleate in unlabeled POPC vesicles (A) compared to the *sn*-1 and *sn*-2 carbonyls of POPC.
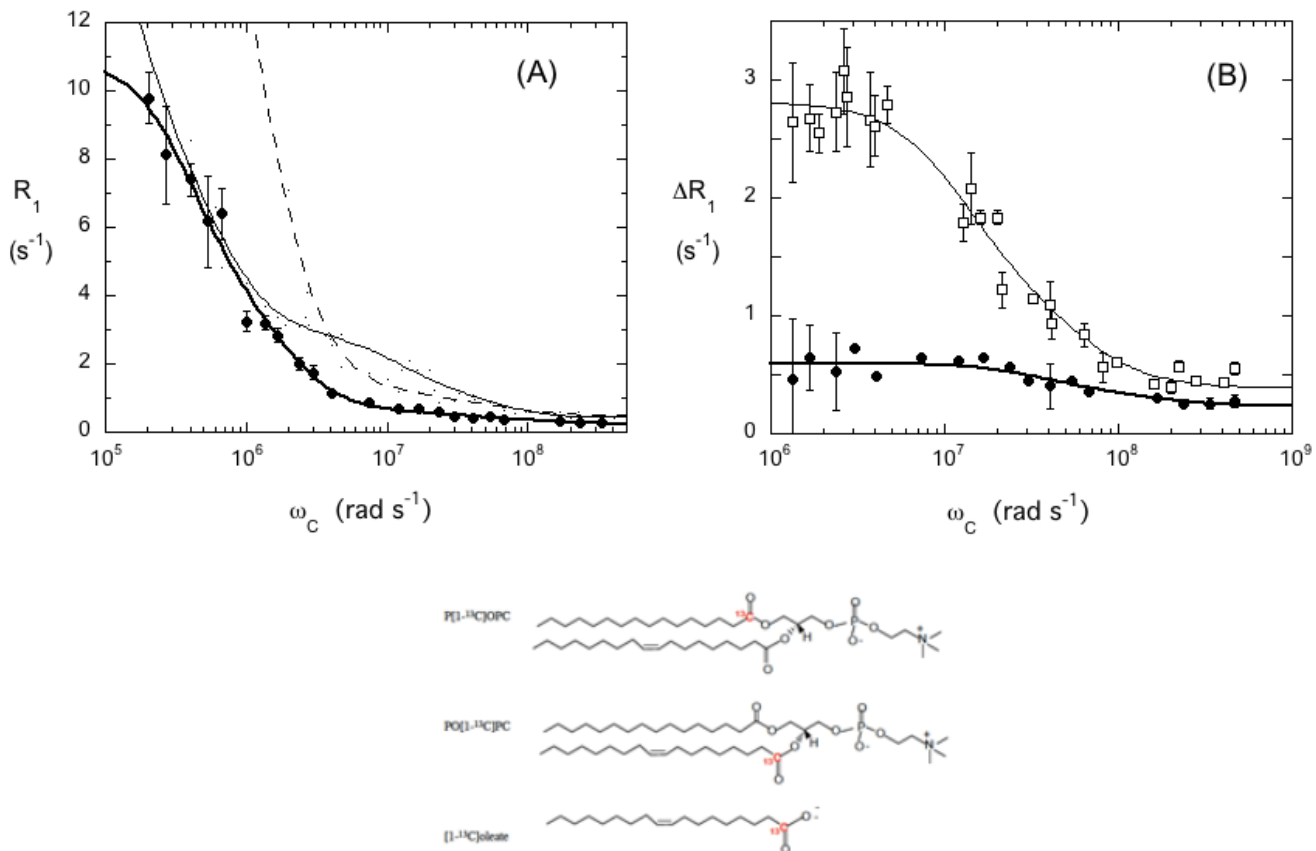
(A) The fits for ^{13}C R_1 versus ω_C for the *sn*-1 (- - - -) and *sn*-2 (———) carbonyls, P[1-^{13}C]OPC and PO[1-^{13}C]PC respectively, are compared to the fit for [1-^{13}C]oleate (filled circle) in oleate/POPC (1:3) SUVs.

(B) Dependence of $\Delta R_1 = R_1 - R_{D0}$ on ω_C for the *sn*-2 ^{13}C (open square) and oleate (filled circle). The data for $\omega_C > 4 \times 10^8$ rad s^{-1} was excluded to avoid the small R_{CSA} contribution so that $\Delta R_1 = R_{D1} + k_{xs}$. The values for τ_{D0}, $R_{D0}(0)$, τ_{D1}, $R_{D1}(0)$, and k_{xs} (equal to $R_{D2}(0)$) are given in Table 1.

Figure S5. ^{31}P field cycling profiles for DOPMe/POPC/cholesterol (1:1:1) SUVs at 40°C (A) The observed R_1 for both phospholipids is shown: POPC (blue squares); DOPMe (red circles). (B) The well-defined R_{D0} has been subtracted from the data and ΔR_1 was fit with $R_{D1}+k_{xs}+R_{CSA}$.
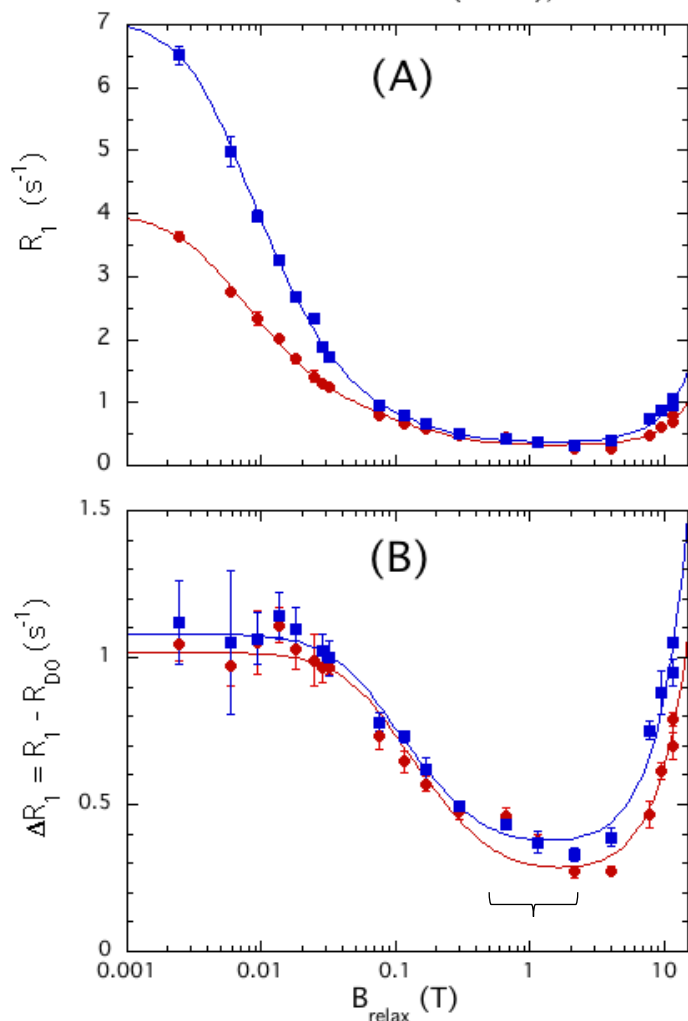
	τ_{D1} (ns)	$R_{D1}(0)$ (s^{-1})	$\tau_D/R_{D1}(0)$ (s^2)	$R_{D2}(0)$ (s^{-1})
DOPMe	30±2	0.75±0.02	4.0x10^{-8}	0.27±0.01
POPC	36±3	0.72±0.03	4.9x10^{-8}	0.36±0.01

The data, from Roberts et al. *Biophys. J.* **2009**, *97*, 132-141, were reanalyzed with $R_1 = R_{D0}+R_{D1}+k_{xs}+R_{CSA}$. The higher temperature was chosen to obtain sufficient data below 0.01 T. The value of $\tau_D/R_{D1}(0)$ is similar to that for headgroup deuterated phospholipids suggesting that the glycerol -CH$_2$OP- interaction is what contributes to R_{D1} with a $\tau_{D1} \sim 30$ μs. The bracket indicates a region that is not well fit and likely has contributions from an R_{D1} specifically for the choline -CH$_2$OP- interaction.

Figure S6. Extracting R_{D2} parameters for the *sn*-2 ^{13}C-labeled POPC data in the high field region containing R_{D1}, R_{D2}, and R_{CSA} and using $\tau_{D2} = 0.08$ ns.
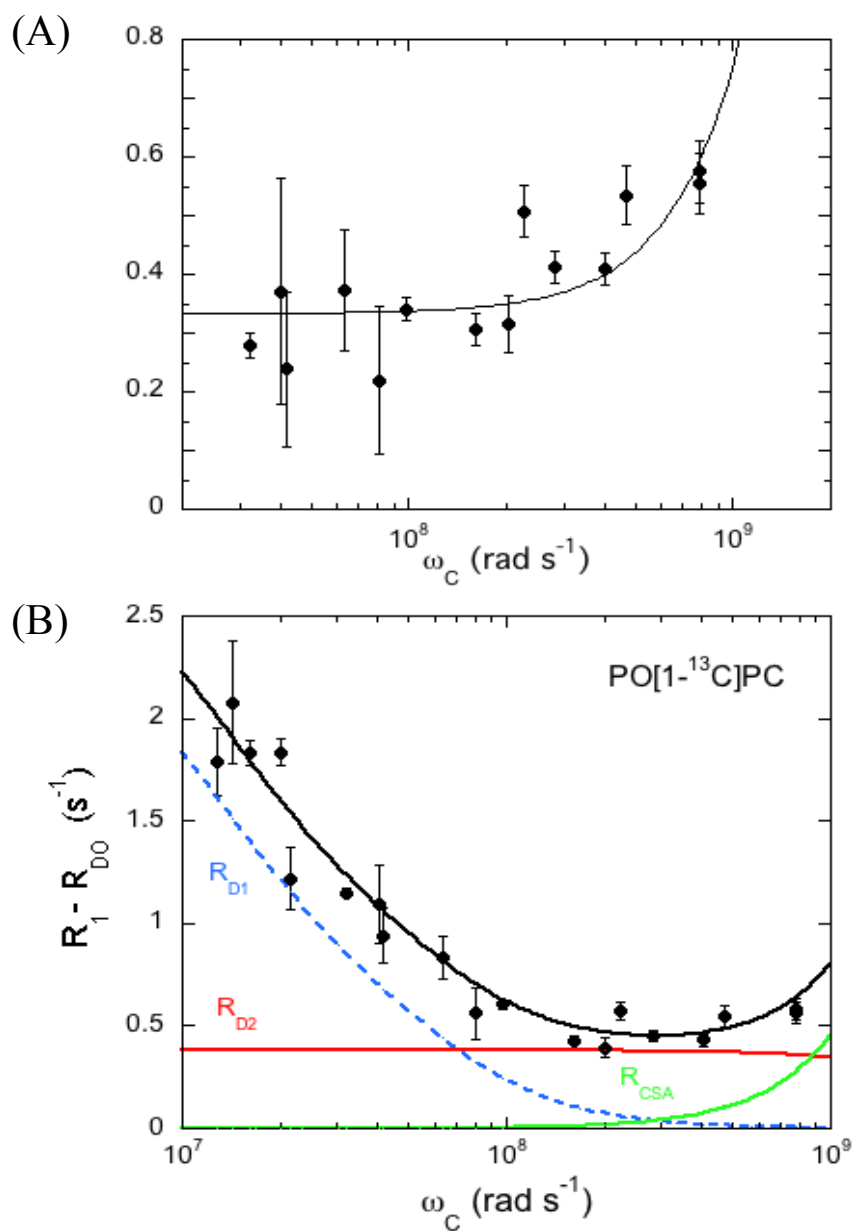
For both (A) and (B), R_{D0} has been subtracted (although it contributes little in this region). In the top R_{D1} has also been subtracted so that the data represent $R_{D2} + R_{CSA}$. In the bottom panel, the data with R_{D1} is shown along with each NMRD shown separately.